DESIGN, SIMULATION, AND FABRICATION OF CUBESAT ANTENNA SYSTEMS

A THESIS SUBMITTED TO
THE GRADUATE SCHOOL OF NATURAL AND APPLIED SCIENCES
OF
MIDDLE EAST TECHNICAL UNIVERSITY

BY

TÜRKER DOLAPÇI

IN PARTIAL FULFILLMENT OF THE REQUIREMENTS
FOR
THE DEGREE OF MASTER OF SCIENCE
IN
ELECTRICAL AND ELECTRONICS ENGINEERING

SEPTEMBER 2020

Approval of the thesis:

DESIGN, SIMULATION, AND FABRICATION OF CUBESAT ANTENNA SYSTEMS

submitted by **TÜRKER DOLAPÇI** in partial fulfillment of the requirements for the degree of **Master of Science in Electrical and Electronics Engineering Department, Middle East Technical University** by,

Prof. Dr. Halil Kalıpçılar
Dean, Graduate School of **Natural and Applied Sciences** _____

Prof. Dr. İlkay Ulusoy
Head of Department, **Electrical and Electronics Engineering** _____

Assoc. Prof. Dr. Özgür Ergül
Supervisor, **Electrical and Electronics Engineering, METU** _____

Examining Committee Members:

Prof. Dr. Sencer Koç
Electrical and Electronics Engineering, METU _____

Assoc. Prof. Dr. Özgür Ergül
Electrical and Electronics Engineering, METU _____

Prof. Dr. Özlem Aydın Çivi
Electrical and Electronics Engineering, METU _____

Prof. Dr. Şimşek Demir
Electrical and Electronics Engineering, METU _____

Assist. Prof. Dr. Ahmed Akgiray
Electrical and Electronics Engineering, Özyeğin University _____

Date: 17.09.2020

I hereby declare that all information in this document has been obtained and presented in accordance with academic rules and ethical conduct. I also declare that, as required by these rules and conduct, I have fully cited and referenced all material and results that are not original to this work.

Name, Surname: Türker Dolapçı

Signature :

ABSTRACT

DESIGN, SIMULATION, AND FABRICATION OF CUBESAT ANTENNA SYSTEMS

Dolapçı, Türker
M.S., Department of Electrical and Electronics Engineering
Supervisor: Assoc. Prof. Dr. Özgür Ergül

September 2020, 82 pages

This study aims to design, simulate, and fabricate on-board and ground station antenna systems for CubeSats, i.e., the most affordable space missions. An on-board UHF turnstile antenna system is optimized in simulation evironment in accordance with different pattern requirements, by changing the orientation of the antenna arms. In order to feed the turnstile antenna arms by successive 90° phase differences between them, a four-way quadrature splitter circuit is designed and fabricated. Antenna pattern measurement is conducted in anechoic chamber by connecting the monopole antenna arms to the fabricated power splitter circuit, while the arms are oriented in the optimized directions and placed on a generic 1U CubeSat platform. In addition to the fabricated UHF turnstile antenna, a novel dual-band V/UHF trapped turnstile antenna involving traps on the antenna arms is designed in simulation environment. On the other side, a circularly polarized VHF ground station Yagi antenna system is designed to achieve optimum gain and size, and it is also fabricated by using low-cost materials to be employed for amateur radios. In addition to the radiating metal structure, the VHF Yagi antenna system includes a Wilkinson power divider and impedance matching baluns fabricated by coaxial transmission lines. Besides the reflection coefficient

measurements, the constructed ground station antenna system is used for the reception of a Slow Scan TV (SSTV) image broadcasted by International Space Station (ISS) to test its functionality. Finally, as another component of a sub-GHz CubeSat ground station, a circularly polarized UHF Yagi antenna system is designed, based on the experience gained from the VHF ground station antenna design and measurement.

Keywords: CubeSat antennas, on-board antennas, ground stations, amateur radio, turnstile antenna, antenna trap, Yagi antennas

ÖZ

KÜP UYDU ANTEN SİSTEMLERİNİN TASARIM, BENZETİM VE ÜRETİMİ

Dolapçı, Türker
Yüksek Lisans, Elektrik ve Elektronik Mühendisliği Bölümü
Tez Yöneticisi: Doç. Dr. Özgür Ergül

Eylül 2020 , 82 sayfa

Bu çalışmada, ulaşması en kolay uzay platformları olan küp uydular için, araç üstü ve yer istasyonu antenlerinin tasarımı, benzetimi ve üretimi amaçlanmıştır. Araç üstü UHF turnike anten sistemi, farklı ışıma örüntüsü gereksinimlerine göre, anten kollarının yönelimlerinin benzetim ortamında değiştirilmesiyle en iyileştirilmiştir. Turnike anten sistemi elemanlarının aralarında 90° faz farkları olacak şekilde beslenmeleri için bir dört yollu, dördün-faz güç bölücü tasarlanmış ve üretilmiştir. Üretilen güç bölücüye monopol anten elemanlarının en iyileştirilen yönelimlerle 1U ölçüsündeki bir CubeSat platformunun üzerindeyken takılmasıyla, ışıma örüntüsü ölçümleri yankısız odada gerçekleştirilmiştir. Üretilen ve ölçümü gerçekleştirilen UHF bandındaki sistemden başka, anten kollarında tıkaçlar içeren yenilikçi bir çift-bant V/UHF tıkaçlı anten sistemi tasarlanmıştır. Diğer tarafta, dairesel polarizasyonlu bir VHF yer istasyonu Yagi anten sistemi, en uygun kazanç ve büyüklük hedefiyle tasarlanmış, amatör telsiz kullanımları doğrultusunda düşük bütçeli malzemelerden imal edilmiştir. Yayın yapan metal yapı, eş-eksenli iletim hatlarının kullanılmasıyla imal edilen Wilkinson güç bölücü ve empedans uyumlayıcı balunlar vasıtasıyla beslenmiştir. Yansıma katsa-

yısı ölçümlerinin yanı sıra, Uluslararası Uzay İstasyonu (ISS) tarafından yayınlanan yavaş taramalı televizyon (SSTV) görüntüsünün üretilen anten yardımıyla alınmasıyla işlevsel testler gerçekleştirilmiştir. Son olarak, VHF anten tasarım ve ölçümlerinden elde edilen tecrübe ile, UHF frekans bandında çalışacak bir Yagi yer istasyonu anten sistemi tasarlanmıştır.

Anahtar Kelimeler: Küp uydu antenleri, araç üstü antenler, yer istasyonları, amatör telsiz, turnike anten, anten tıkacı, Yagi antenler

To Ece

ACKNOWLEDGMENTS

First of all, I would like to thank my supervisor, Assoc. Prof. Dr. Özgür Ergül, for his support and guidance, since 2015. Thanks to him, in addition to electromagnetics, I learnt how to conduct scientific research, decently. I am obliged he has given a chance to me to work with him.

Other than my supervisor, I would like to thank Prof. Dr. Özlem Aydın Çivi and Prof. Dr. Şimşek Demir, who taught me the fundamentals of my profession, and Prof. Dr. Sencer Koç, who spent time with me in the anechoic chamber to test my thesis study, in addition to his contributions to my engineering life with the courses he taught. It is a privilege for me that they accepted to be the members of my thesis examination committee, together with Assist. Prof. Dr. Ahmed Akgiray, who is a valuable engineer and academician.

I am grateful to TAMSAT members, who make the dreams come true. Without them, it would be impossible to realize the designs. Special thanks go to Baran Akbıyık, Eralp Göğen, Emre Karamullaoğlu, Şahin Küliğ, Prof. Dr. Yıldırım Sara, Koray Toksöz, and, the pioneer A. Tahir Dengiz (TA2T, SK), who will always be remembered. We will continue to follow the way he left behind to improve ourselves and to make the space technology accessible to everyone.

Without CEMMETU research group's contribution and inspiration, this thesis study wouldn't be progressed. I am lucky to have awesome apprentices, M. Sezgin Baloğlu, who collaborated with me to design antennas with unconventional materials, and M. Barış Şahin, who collaborated with me to design CubeSat antennas. They spend time with me with a great willingness of learn.

I am thankful to TÜBİTAK 2210A National Scholarship Program, who supported me in my graduate studies.

Special thanks to Amphenol RF, Hilitron Technologies, Innovative Power Products,

Matec Electronics, Mini Circuits, Rohde & Schwarz, Times Microwave, and Würth Elektronik, who supported this work by providing free samples and demo products. Also, I would like to thank Magnetron Defence & Space, PRF ArGe, and Somyaz Bilişim Teknolojileri, where I spend some hours to use their measurement equipments and fabrication facilities.

My deepest gratitude goes to Ece Alpuğan, who was always by my side with her love and encouragement, even in the last days of her life. She will always be remembered with her kindness. May she rest in peace.

Last but not least, I would like to thank my family and friends, who motivated me in my journey of learning. I am sure they won't let me down, when I ask their help to continue this endless journey.

TABLE OF CONTENTS

ABSTRACT v

ÖZ vii

ACKNOWLEDGMENTS x

TABLE OF CONTENTS xii

LIST OF TABLES xv

LIST OF FIGURES xvi

CHAPTERS

1 INTRODUCTION 1

1.1 Small Satellite Types and CubeSat Standards 2

1.2 Subsystems of a CubeSat 4

1.3 Consideration of Link Margin 7

1.4 Scope and Organization of the Thesis 7

2 ON-BOARD ANTENNA SYSTEMS 9

2.1 Sub-GHz On-Board Antenna Literature and Market Review 10

2.2 UHF Circularly Polarized On-Board Antenna Configuration: Turnstile Antenna 14

2.2.1 Background on Turnstile Antennas 15

2.2.2 Design and Simulation of Radiating Structure 16

2.2.3 Design and Simulation of Feed Circuit 28

2.2.4 Fabrication and Measurement 32

2.3 V/UHF Circularly Polarized On-Board Antenna Configuration: Dual-band Trapped Turnstile Antenna 36

2.3.1 Background on Antenna Trapping and Design of a V/UHF Trapped Dipole Antenna 37

2.3.2 Design of Dual-Band Trapped V/UHF Turnstile Antenna . . . 40

3 GROUND STATION ANTENNA SYSTEMS 43

3.1 Antenna Types and Selection Criteria 45

3.2 Design and Fabrication of a Directive Antenna: Circularly Polarized VHF Yagi Antenna 46

3.2.1 Background on Yagi Antenna 47

3.2.2 Design Specifications 49

3.2.3 Block Level System Design 50

3.2.4 Design and Simulation of the Radiating Structure 52

3.2.5 Design and Simulation of the Feed Structure 56

3.2.5.1 Impedance Matching Balun: Quarter-Wave Transformer with Ferrite Bead 57

3.2.5.2 Wilkinson Power Divider 61

3.2.5.3 Combined Feed Structure: Power Divider and Impedance Matching Balun 64

3.2.6 Fabrication and Measurement 66

3.2.7 Field Test 69

3.3 Design of a Circularly Polarized UHF Yagi Antenna 69

4 CONCLUSIONS AND FURTHER WORKS 73

REFERENCES 77

LIST OF TABLES

TABLES

Table 2.1 Properties of on-board antenna candidates. 14

Table 3.1 Optimized design parameters for Yagi arrays to achieve different gain values [54]. 48

Table 3.2 VHF directive antenna design specifications. 50

Table 3.3 Fabricated VHF Circularly Polarized Yagi antenna. 55

Table 3.4 Designed UHF Circularly Polarized Yagi antenna. 72

LIST OF FIGURES

FIGURES

Figure 1.1 Total numbers of small satellite launchs [4]. 2

Figure 1.2 1U and 3U CubeSats [7]. 3

Figure 1.3 Poly-Picosatellite Orbital Deployer (P-POD) [8]. 4

Figure 1.4 Galassia-2 CubeSat[9]. 5

Figure 1.5 Downlink operation frequencies of small satellites [4]. 6

Figure 2.1 A generic CubeSat's transceivers and antennas. 10

Figure 2.2 Tape measure V-dipole antenna [19]. 11

Figure 2.3 GOMSpace UHF turnstile antenna system [21]. 12

Figure 2.4 ISIS Space hybrid antenna system consisting of a VHF dipole and a UHF monopole [20]. 13

Figure 2.5 A turnstile antenna [33]. 15

Figure 2.6 Generic antenna module feed circuit, which supports up to four arms. 17

Figure 2.7 The mechanical model of the UHF turnstile antenna with no rotation or tilt of antenna arms. 18

Figure 2.8 Gain of the UHF turnstile antenna with no rotation or tilt of antenna arms. 18

Figure 2.9 Optimum selection criteria sets to evaluate the results of the turnstile antenna parametric study. 19

Figure 2.10 Gain of the UHF turnstile antenna at $\theta = 0°$, $\phi = 0°$ with different arm rotation and arm tilt angles. 20

Figure 2.11 $AR < 3$ dB beamwidth of the UHF turnstile antenna at the upper hemisphere with different arm rotation and arm tilt angles. 21

Figure 2.12 The mechanical model of the UHF turnstile antenna with $-45°$ arm rotation angle and $90°$ arm tilt angle, which results in a RHCP directive radiation pattern towards $\theta = 0°$. 21

Figure 2.13 Gain of the UHF turnstile antenna with $-45°$ arm rotation angle and $90°$ arm tilt angle. 22

Figure 2.14 Gain of the UHF turnstile antenna at $\theta = 180°$, $\phi = 0°$ with different arm rotation and arm tilt angles. 22

Figure 2.15 $AR < 3$ dB beamwidth of the UHF turnstile antenna at the lower hemisphere with different arm rotation and arm tilt angles. 23

Figure 2.16 The mechanical model of the UHF turnstile antenna with $45°$ arm rotation angle and $90°$ arm tilt angle, which results in a LHCP directive radiation pattern towards $\theta = 180°$. 23

Figure 2.17 Gain of the UHF turnstile antenna with $45°$ arm rotation angle and $90°$ arm tilt angle. 24

Figure 2.18 Gain difference between $\theta = 0°$ and $\theta = 180°$ of the UHF turnstile antenna with different arm rotation and arm tilt angles. 24

Figure 2.19 The mechanical model of the UHF turnstile antenna with $-15°$ arm rotation angle and $60°$ arm tilt angle, which results in minimum gain difference between $\theta = 0°$ and $\theta = 180°$. 25

Figure 2.20 Gain of the UHF turnstile antenna with $-15°$ arm rotation angle and $60°$ arm tilt angle. 25

Figure 2.21 Minimum gain of the UHF turnstile antenna with different arm rotation and arm tilt angles. 26

Figure 2.22 The mechanical model of the UHF turnstile antenna with 0° arm rotation angle and 75° arm tilt angle, which results in a maximized minimum gain value. 26

Figure 2.23 Gain of the UHF turnstile antenna with 0° arm rotation angle and 75° arm tilt angle. 27

Figure 2.24 Percentage of the radiation areas with $AR < 3$ dB for the UHF turnstile antenna with different arm rotation and arm tilt angles. 27

Figure 2.25 Design of the four-way quadrature splitter with ideal blocks. . . 29

Figure 2.26 EM simulation layout of the UHF turnstile antenna feed circuit. 30

Figure 2.27 EM simulation results of the UHF turnstile antenna feed circuit. 31

Figure 2.28 Fabricated and assembled antenna feed circuit. 32

Figure 2.29 Measurement results of the UHF turnstile antenna feed circuit. . 33

Figure 2.30 The antenna prototype placed in the anechoic chamber. 34

Figure 2.31 Monopole antenna tuning with aluminum tape. 35

Figure 2.32 Measurement and simulation results for the radiation pattern. . . 35

Figure 2.33 Normalized gain obtained with different polarization directions of the linearly polarized measurement antenna. 36

Figure 2.34 Trapped monopole antenna [38]. 37

Figure 2.35 Trapped dipole antenna modeled in 4NEC2. 38

Figure 2.36 Impedance values of the designed trap at different frequencies. . 39

Figure 2.37 Reflection coefficient simulation result for the trapped dipole antenna in 4NEC2. 39

Figure 2.38 Radiation pattern simulation results for the trapped dipole antenna in 4NEC2 at 145.5 MHz (left) and 436.5 MHz (right). 40

Figure 2.39 Reflection coefficient result for an antenna arm of the V/UHF turnstile antenna without any rotation or tilt. 41

Figure 2.40 Gain of the V/UHF turnstile antenna without any rotation or tilt at 145.5 MHz. 41

Figure 2.41 Gain of the V/UHF turnstile antenna without any rotation or tilt at 436.5 MHz. 42

Figure 3.1 A simple ground station system (SPDT: Single-pole, double-throw switch). 44

Figure 3.2 Yagi antenna with N elements [53]. 47

Figure 3.3 Circularly polarized Yagi antenna feed. 51

Figure 3.4 Circularly polarized Yagi antenna modeled in ANSYS HFSS. . . 52

Figure 3.5 Gain of the initial design at different frequencies. 53

Figure 3.6 Gain at 145.5 MHz for different design frequencies. 54

Figure 3.7 Gain simulation of the VHF Yagi prepared for fabrication. 54

Figure 3.8 Simulated reflection coefficient curves for the VHF Yagi antenna prepared for fabrication with different feed arm lengths. 55

Figure 3.9 VHF Yagi simulation on top of the infinite ground plane. 56

Figure 3.10 Transmission line terminated with a load [58]. 57

Figure 3.11 Quarter-wave transformer simulation model. 59

Figure 3.12 Quarter-wave transformer simulation results. 59

Figure 3.13 Currents on a coaxial fed dipole antenna [51]. 60

Figure 3.14 Snap-on ferrite beads [60]. 60

Figure 3.15 Two-way Wilkinson power divider. 61

Figure 3.16 Half-circuits for (a) even excitation, (b) odd excitation [58]. . . . 61

Figure 3.17 Wilkinson power divider simulation model. 63

Figure 3.18 Wilkinson power divider simulation results. 63

Figure 3.19 Overall system simulation model. 64

Figure 3.20 Overall system simulation results. 65

Figure 3.21 Prepared mask for the Wilkinson power divider PCB. 66

Figure 3.22 Fabricated Wilkinson power divider. 67

Figure 3.23 Wilkinson power divider measurement results. 67

Figure 3.24 Fabricated impedance matching balun. 68

Figure 3.25 Fabricated Yagi antenna on a tripod. 68

Figure 3.26 Measurement results for the fabricated Yagi antenna. 69

Figure 3.27 ISS pass details for OSTİM, Ankara on 05.08.2020 [61]. 70

Figure 3.28 Received SSTV image. 70

Figure 3.29 Gain simulation of the designed UHF Yagi antenna. 71

Figure 3.30 Reflection coefficient simulation results for the designed UHF Yagi antenna. 71

CHAPTER 1

INTRODUCTION

To conduct space research with military, commercial or scientific purposes, satellites are used. Several research fields, e.g., electronics, telecommunications, biology, positioning, remote sensing, and imaging, require low-cost prototyping platforms for proof-of-concept in the space environment. It is known that the unit cost of launching a traditional satellite is not less than $\$65.000.000$, even with efficient use of resources [1]. This high cost limits space research activities, especially for non-commercial scientific purposes. However, a launch of a small satellite of 3U ($10 \times 10 \times 30$ cm) costs $\$295.000$ [2], which is a very reasonable amount when compared to traditional satellite launches. With the help of easy-to-reach durable components and DIY culture, university students all around the world take part in space research thanks to such low-cost small satellite projects. In addition to scientific and educational purposes, possibility of a satellite swarm with small units is highly attractive in military[3].

Easy-to-reach, low-cost platforms have become widespread in the last years. According to [4], more than 1000 small satellites (class nanosatellite) are orbiting Earth, and half of them are launched in the last two years. Over 3000 small satellite missions are forecasted for the next six years. Related plot taken from [4] can be seen in Figure 1.1.

In this thesis, it is aimed to develop on-board and ground station antennas for CubeSat systems, which are the most popular types of small satellites. In this introductory chapter, fundamental information on CubeSats are included, by summarizing their subsystems. At the end of the chapter, the organization of this thesis is presented.

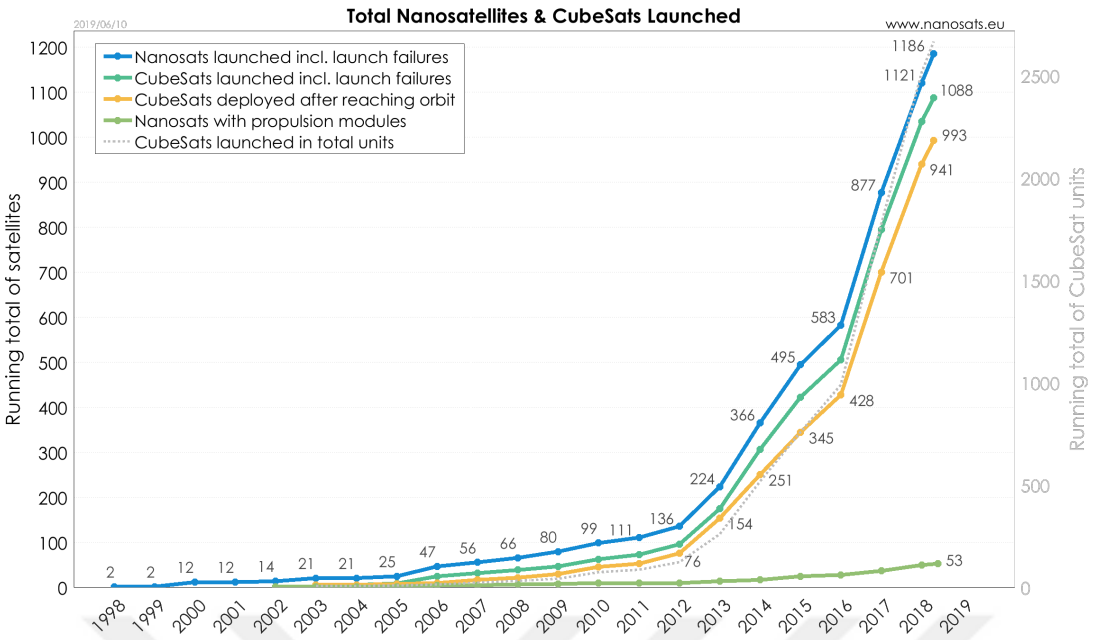
Total Nanosatellites & CubeSats Launched
2019/06/10
www.nanosats.eu
Nanosats launched incl. launch failures
CubeSats launched incl. launch failures
CubeSats deployed after reaching orbit
Nanosats with propulsion modules
CubeSats launched in total units
Running total of satellites
Running total of CubeSat units
1200
1100
1000
900
800
700
600
500
400
300
200
100
0
2500
2000
1500
1000
500
0
2 2 12 12 14 21 21 25 47 56 66 80 99 111 136 224 366 495 583 877 1121 1186
2 2 12 12 14 21 21 25 47 56 66 80 99 111 136 224 366 495 583 877 1088
2 2 12 12 14 21 21 25 47 56 66 80 99 111 136 224 366 495 583 701 941 993
2 2 12 12 14 21 21 25 47 56 66 80 99 111 136 154 251 345 428 701
2 2 12 12 14 21 21 25 47 56 66 80 99 111 136 154 251 345 428 583 877 1121 1186
2 2 12 12 14 21 21 25 47 56 66 80 99 111 136 154 251 345 428 583 877 1088
2 2 12 12 14 21 21 25 47 56 66 80 99 111 136 154 251 345 428 583 701 941 993
2 2 12 12 14 21 21 25 47 56 66 80 99 111 136 154 251 345 428 583 701

mechanical pieces at the outer side of the satellite. The aim of this standardization is to decrease the cost of transportation to space with standard deployer systems designed to comply with launch vehicles. 1U and 3U CubeSats of Cal Poly can be seen in Figure 1.2 [7], while a deployer, which is an interface between a CubeSat and a launch vehicle that carries a CubeSat to its orbit, is shown in Figure 1.3 [8].

Figure 1.2: 1U and 3U CubeSats [7].

Figure 1.3: Poly-Picosatellite Orbital Deployer (P-POD) [8].

1.2 Subsystems of a CubeSat

Subsystems of a CubeSat can be investigated under two classes. The first group includes the compulsory subsystems for the CubeSat to operate, while the second group includes optional payloads for specific mission purposes. It is both possible for a CubeSat project team to fabricate the subsystems in-house or to use readily fabricated subsystems from commercial suppliers. Usually, project teams prefer designing specific subsystems by themselves, while buying the rest of the subsystems (generally with space heritage) from suppliers. This section summarizes the subsystems of a typical CubeSat in a generic manner.

A photograph showing the subsystems of a CubeSat developed by the National University of Singapore, namely Galassia-2 is shown in Figure 1.4 [9]. The mission of Galassia-2 is to conduct multispectral imaging for remote sensing of agricultural and environmental changes. There is not detailed technical information given in the mission website, but Figure 1.4 [9] includes sufficient information to give this system as an example to explain generic CubeSat subsystems.

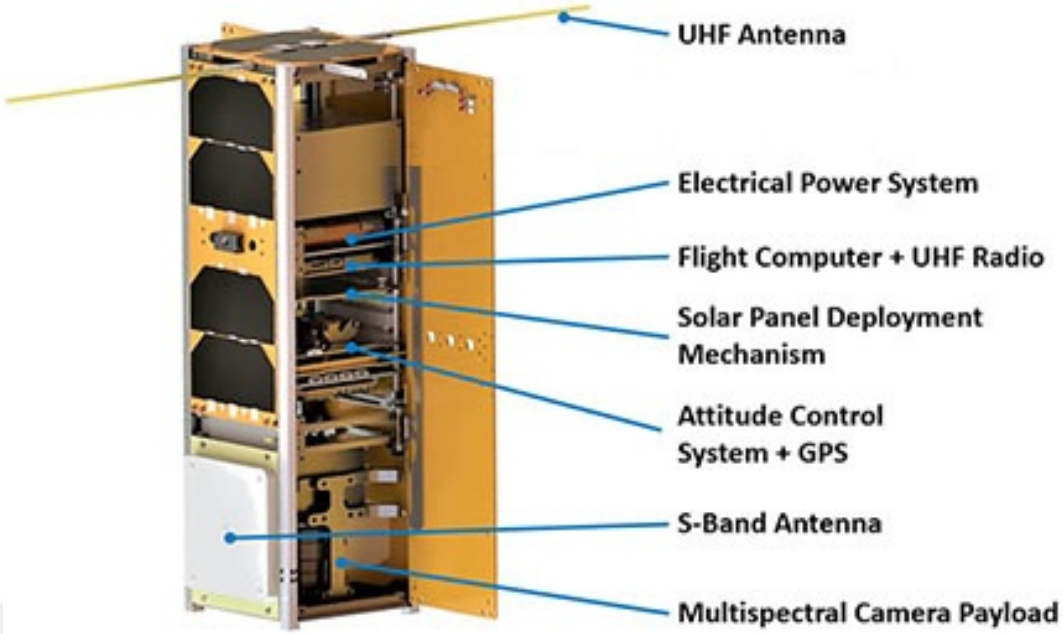

Figure 1.4: Galassia-2 CubeSat[9].

A CubeSat maintains its operation by converting solar energy into electrical energy with the help of solar panels. Generally, most of the sides of a CubeSat are covered by solar panels to maximize the capture of the solar energy. In some missions, there are deployable mechanisms to increase the area with solar panels. The solar power is used for charging the batteries of the CubeSat. Battery charge, power regulation, and distribution operations are conducted by the Electrical Power System (EPS).

Most of the CubeSats do not have any propulsion system, because of the difficulties in terms of energy consumption, mechanical integration, and electromagnetic interference (EMI) [10]. Despite the lack of propulsion, it is still possible to align a CubeSat to desired directions for specific requirements, e.g., to conduct high data-rate communication with a ground station by a patch antenna or to take photographs of the Earth. Passive and/or active magnetic attitude control subsystems are used for an alignment with the Earth's magnetic field. Attitude control systems determine the location and orientation of the platform, together with the global positioning system (GPS) receivers [11].

Flight Computer, or On-Board Computer (OBC), is the main processing unit of a

platform. It is the subsystem that monitors and controls all other subsystems. Battery management, watchdog operation, payload operation control, etc. are conducted by OBC. Generally, system status messages are transmitted by a beacon signal continuously or at discrete events, according to the configuration. Sometimes it is possible to change the settings of a CubeSat with an uplink command signal from a ground station, by reaching the OBC remotely. Single or multiple transceiver systems are included in platforms for different purposes.

CubeSat operation frequencies are generally selected as one of the amateur or Industrial Scientific Medical (ISM) bands. In Figure 1.5, a plot taken from [4] shows a statistical data of downlink frequency selections. Downlink beacon signals, which require a narrow bandwidth, are transmitted to ground stations in the UHF frequency band, whereas the outputs of payloads (such as image data) that require much more bandwidth are transmitted to ground stations at higher frequencies, such as in S or X frequency bands. Although there is no statistical data showing uplink frequency selections, as used in [12], [13], [14], they are generally in VHF amateur band, at around 145 MHz. So, there are mostly more than one antenna in a CubeSat to maintain GPS, main uplink operation, main downlink operation, and payload operations.

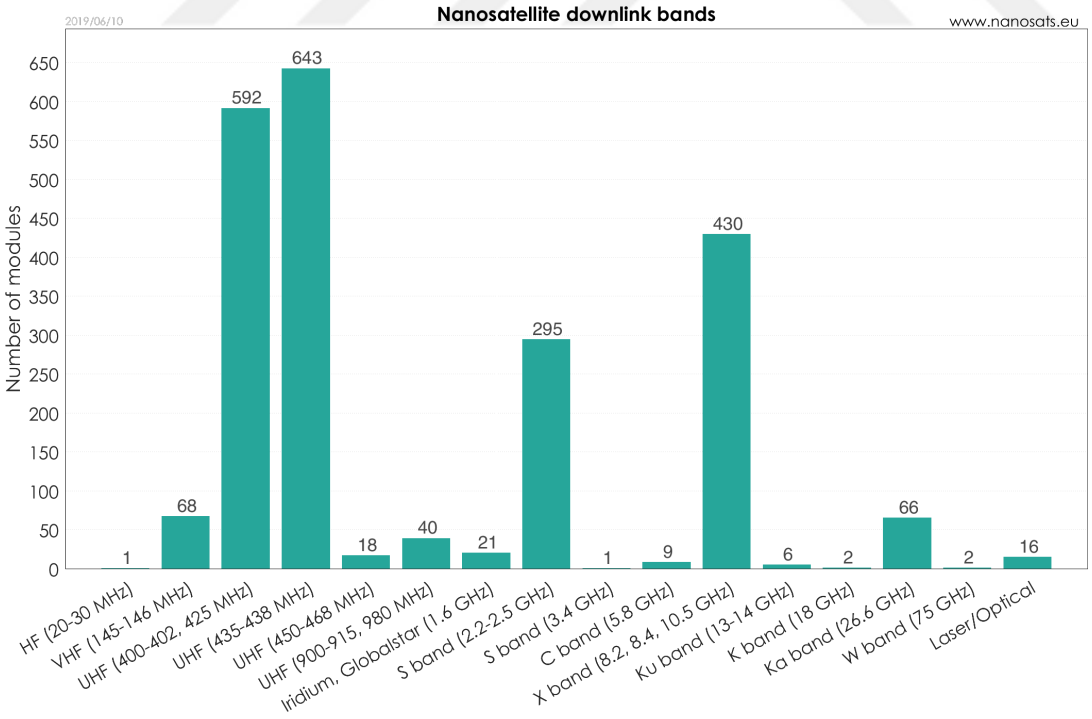

Figure 1.5: Downlink operation frequencies of small satellites [4].

1.3 Consideration of Link Margin

According to the link budget analysis presented in [15], by using 1 W and 100 W transmitters on CubeSat and its ground station, respectively, antennas with 2.2 dBi gains make the link margin positive in both VHF and UHF frequency bands, considering a communication link using AX.25 protocol with 20 kHz bandwidth that requires 6.3 dB SNR for a proper operation. The weakest side of the communication link is the limited output power of the CubeSat transmitter. To continue operation in the case of additional losses, such as unexpected plumbing loss, atmospheric loss, depointing loss, cross polarization discrimination, etc., an additional link margin is required. This can be obtained by increasing the antenna gains or decreasing the losses in the link budget. For example, polarization loss can be prevented by using circularly polarized antennas and the received power can be increased by using antennas with higher gain values. Optimum specifications are determined by project teams to obtain the highest gain margin with available resources.

1.4 Scope and Organization of the Thesis

This study includes all development steps of CubeSat antennas in detail for both on-board systems and ground station systems, including their design, simulation and fabrication. For the on-board side, we consider turnstile antenna systems, which contain quadrifilar phasing structures. Design and fabrication of an UHF turnstile antenna system is followed by the design of a novel dual-band trapped V/UHF turnstile antenna system. On the ground station side, we focus on circularly polarized Yagi antennas. The thesis study is planned to meet the requirements of Turkish Amateur Satellite Organization (TAMSAT), which aims to design CubeSat and ground station systems for scientific and educational aerospace missions without any commercial concern.

Thesis is organized as separate chapters for on-board and ground station antenna systems. Each chapter includes both background information and design steps, followed by fabrication and measurement results. Thesis is finalized by a conclusion chapter, by discussing the results and planning the future studies.

CHAPTER 2

ON-BOARD ANTENNA SYSTEMS

Antennas play important roles on CubeSat platforms, which transmit and receive radio waves for different purposes, such as broadcasting, communication, telemetry, and telecommand operations. As mentioned in Chapter 1, a CubeSat may have a single antenna or multiple antennas according to the requirements of its mission and mechanical restrictions. Sub-GHz frequencies are used for low data rate telemetry, telecommand, voice transmission, and SSTV operations, whereas higher frequency bands are used for transmissions of large amounts of payload data, such as high-resolution images [16]. As challenging requirements, on-board antennas have strict size limitations in accordance with CubeSat standards. In the frequency bands with lower frequencies, such as VHF and UHF, size limitations become very critical, due to longer operation wavelengths, when compared to bands with higher frequencies. Deployment mechanisms that hold antennas in a compartment till the release of the platform to the space are typically used for wire antennas that extend from the platform to outside. Also, it is important to design the platform in a way to maximize the reception of the solar energy, without trading off antenna area for solar panel area or interfering the sunlight on solar panels [17]. By considering physical constraints, the aim is to optimize gain patterns in the desired directions or to design the most isotropic pattern as much as possible.

In Figure 2.1, a block diagram of a generic CubeSat transceiver system with its antennas is given, assuming that the objective of the mission is to send aerial images captured by the CubeSat to the ground station. In this diagram, the downlink frequency used for sending the telemetry data to the ground station is in the UHF band, while the uplink frequency used for receiving telecommand messages from the ground station

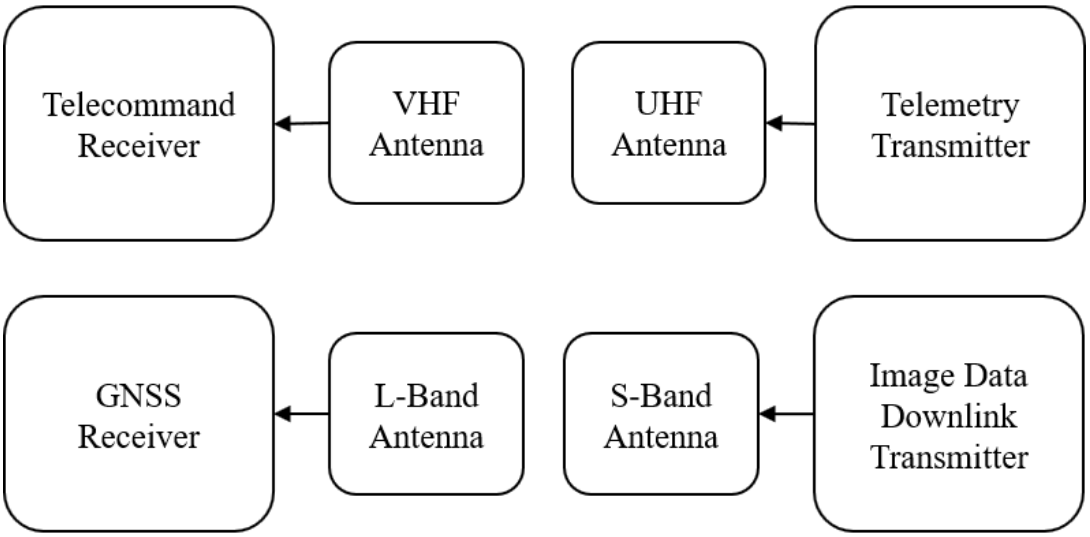

Figure 2.1: A generic CubeSat's transceivers and antennas.

is in the VHF band. In addition, a GNSS receiver is used for receiving timing and position data, and a downlink data transmitter is used for sending images captured by the camera payload in the S Band. On the top of this generic scenario, a CubeSat may include other payloads, such as a radar working in the Ka-Band, which requires an additional antenna on board [18].

Antenna designs or selections among commercial off-the-shelf products are performed by project teams considering mission requirements and available resources. There are many examples in the literature in the context of different scenarios. The study presented in this chapter focuses on on-board antenna systems, putting an emphasis on VHF and UHF systems. The first section reviews some examples in the literature. Then, design and simulation results for a UHF turnstile antenna with a quadrifilar feeding mechanism is presented in the second section. Finally in the third section, a novel dual-band trapped V/UHF turnstile antenna system design is presented.

2.1 Sub-GHz On-Board Antenna Literature and Market Review

VHF and UHF antenna systems are based on whip radiators with several configurations, which are monopole, dipole, and turnstile, in general. An interestingly simple solution for a single-band antenna is to use steel tape measure as the radiating ele-

Figure 2.2: Tape measure V-dipole antenna [19].

ment to form a monopole or a dipole structure. Figure 2.2 shows a V-dipole antenna together with a coaxial balun built in Cornell University, designed to be used in a CubeSat mission [19]. The objective of the bend that leads a V shape rather than a linear structure is to optimize the radiation pattern of the antenna, by decreasing the depth of the nulls.

Commercial products for VHF and UHF antenna systems are distinguished from simple solutions by providing more complex feed mechanisms and internal mechanical deployment subsystems, such as deployable four arm antenna systems. Generally, suppliers provide mechanical structures for systems with up to four antenna arms, which may have different configuration options. The possibilities include separate dipole antennas for VHF and UHF bands, a VHF dipole antenna and a UHF monopole antenna, a turnstile antenna for VHF band, etc. [20]. The main idea in these products is that each arm supports a single frequency, while frequency diversity is maintained by placing arms with different lengths that resonate at different frequencies in a single mechanical structure. By using more than one arm for the same frequency band, it is aimed to optimize gain or axial ratio patterns. A VHF canted turnstile antenna

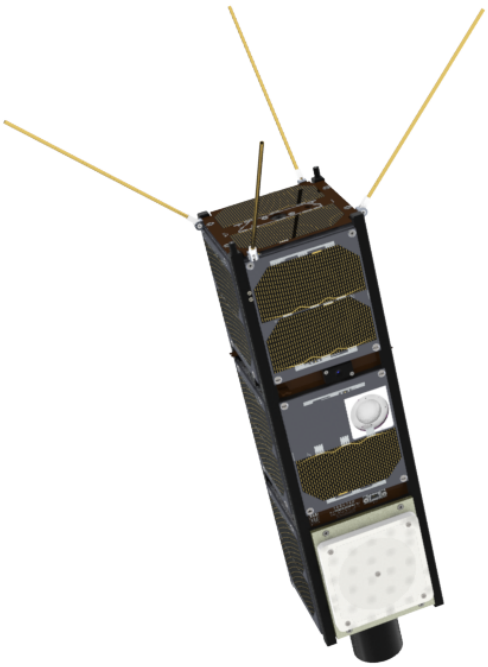

Figure 2.3: GOMSpace UHF turnstile antenna system [21].

product, which includes four tilted monopole elements with 90° successive feeding phases at four sides, provided by GOMSpace is given in Figure 2.3 [21]. Similarly, a combination of a VHF dipole and a UHF monopole provided by ISIS Space is given in Figure 2.4. The configuration of VHF dipole together with UHF monopole leads to linearly polarized antennas at both frequencies, whereas the turnstile configuration leads to a circularly polarized antenna at a single frequency.

Other than simple solutions and widely used commercial products, there are several academic studies, including articles and thesis works that aim to fabricate in-house on-board antenna systems for university missions, review the issues from different viewpoints, or propose novel designs. For example, [22] states that mission objectives determine the structure of the antenna system, and, when combining several antennas, a thorough study is required in order to prevent pattern nulls. The article further presents the usage of a quadrifilar helix antenna in satellites, in which a phase shifting structure is used for circular polarization. A helix antenna in the UHF frequency band with a deployment structure is presented in [23]. In addition to helix, whip, and turnstile antennas for sub-GHz bands, [24] reviews the literature on reflectors,

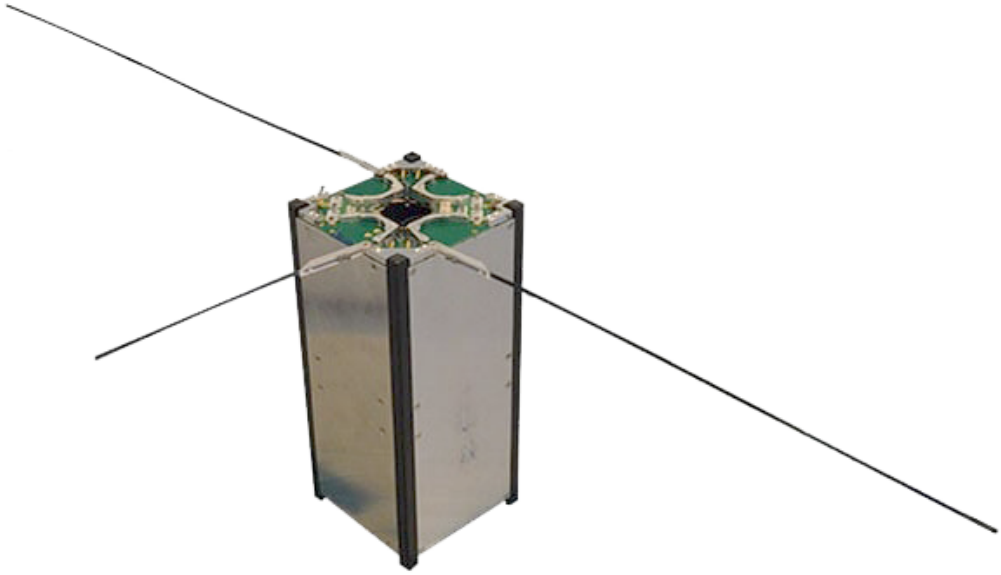

Figure 2.4: ISIS Space hybrid antenna system consisting of a VHF dipole and a UHF monopole [20].

reflectarrays, and horn antennas for high frequencies. As another remarkable study, [25] includes the usage of composite tape springs to enhance the physical flexibility of whip antennas. Using a patch antenna by trading off the solar panel area is preferred in [26], in which an omnidirectional compact UHF antenna is presented.

Norwegian University of Science and Technology Test Satellite (NUTS) project is an interdisciplinary work of graduate students from different areas to design the modules of a CubeSat as their thesis studies. Antenna system proposed in a related thesis is composed of two turnstile antennas, one of which works in the VHF band and the other in the UHF band, while both with narrow bandwidths [27]. The selection of turnstile is due to its circular polarization. The thesis mostly focuses on antenna feeding mechanisms, which give the required phase differences to the arms of the turnstile. Also, the study provides information on balun structures.

Petite Amateur Navy Satellite (PANSAT) is an ancestor of CubeSat projects; it was carried out in Naval Postgradute School in 1990s [28]. This project's antenna section involves three MS theses, which are about the design of an antenna system using Numerical Electromagnetic Code (NEC) [29], optimization of the initial design [30], and finalization and integration of the system [31]. The resulting PANSAT antenna

Table 2.1: Properties of on-board antenna candidates.

Antenna	**Radiation Pattern**	**Polarization**	**Deployment Complexity**	**Solar Panel Area Reduction**
Dipole	Omnidirectional	Linear	Low	Low
Monopole	Omnidirectional	Linear	Low	Low
Axial Mode Helix	Directive	Circular	High	High
Patch	Omnidirectional or Directive	Linear or Circular	N/A	High
Turnstile	Isotropic or Omnidirectional or Directive	Circular	Low	Low

system, which is a tangential canted turnstile structure, is optimized for gain and polarization patterns at a single frequency in the UHF band by the selection of antenna positions and orientation angles. The gain objective of the optimization study is specified as "a pattern with no nulls below -10 dBi". We note that one of the most detailed studies on sub-GHz antennas of small satellites was performed for PANSAT, before the standardization of CubeSats.

One of the few studies aiming to design a dual-band circularly polarized antenna system [32] makes use of two separate phasing structures for VHF and UHF frequencies, while the antenna arms are connected to these separate circuits by using diplexers. The arms are simple whips, and diplexers are designed to optimize matching at both frequencies. It is seen that, due to the use of different lengths of antenna arms in terms of wavelength, the radiation patterns of the antenna system in different frequency bands are not similar to each other.

Commonly used on-board antenna types are compared in Table 2.1 in terms of their main properties.

2.2 UHF Circularly Polarized On-Board Antenna Configuration: Turnstile Antenna

A turnstile antenna in the UHF band is designed and constructed as an on-board antenna module for an 1U CubeSat system. This selection is due to its circular polarization and high gain when compared to monopole and dipole antennas, which are linearly polarized and omnidirectional. Instead of defining numerical specifications to start the design, the limits of this antenna type are first observed by optimiza-

tion sweeps in a simulation environment. The feed circuit of the turnstile antenna is designed, simulated, and prepared for fabrication in NI AWR design and simulation environment. The radiating structure is designed and optimized by changing the orientation of the arms of the antenna module in ANSYS Electronics Desktop simulation environment. The experience gained from this part is used in the design of a dual-band antenna structure, which is presented in the next section.

2.2.1 Background on Turnstile Antennas

A turnstile antenna is a circularly polarized whip antenna configuration that consists of two perpendicularly placed dipole antennas. Circular polarization is obtained by inserting 90° phase difference between the dipoles, either by a physical quarter wavelength separation or by a phase shift of 90° between the feeds of the dipoles, as shown in Figure 2.5 [33]. In [32] phase quadrature is obtained by phase shifters, whereas in [34] and [35], phase quadrature is obtained by the input impedances of the dipoles being complex conjugates of each other. A turnstile antenna can also be constructed as a configuration with four monopoles with successive 90° phase differences between them.

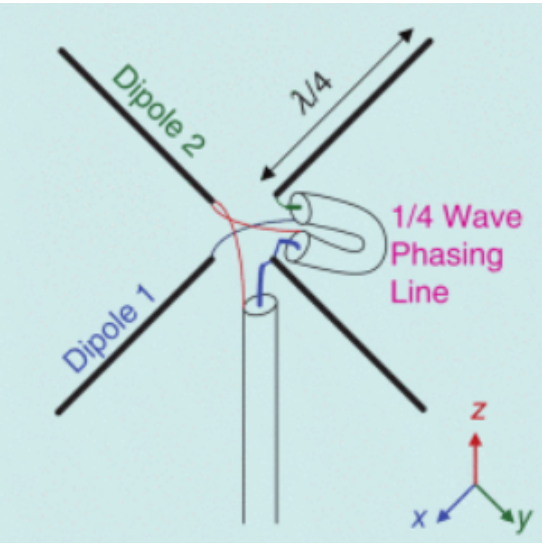

Figure 2.5: A turnstile antenna [33].

The importance of circular polarization in space communications is due to the aim of minimization of the polarization loss. Because of the changing orientation of a CubeSat platform with respect to the ground station, a linearly polarized antenna might cause significant losses in the link budget [36]. Other than their circular polarization, turnstile antennas have gain advantage, when compared to the monopole and dipole antennas that are omnidirectional. A turnstile antenna can be designed to radiate in a desired direction, by the optimization of the orientations of the antenna arms with respect to each other and the platform [30].

In this section, design, simulation, and fabrication of a UHF turnstile antenna on a 1U CubeSat platform is presented. The objective of this study is to realize an antenna prototype, which is to be updated in a further study with the addition of a deployment mechanism and the optimization of the antenna performance. In addition to the UHF design, a novel design which supports V/UHF dual-band operation is presented in the last section of this chapter.

2.2.2 Design and Simulation of Radiating Structure

The radiating structure is designed in ANSYS Electronics Desktop simulation environment, by parametric simulations. A rectangular PEC plate, which has 1.6 mm thickness and 100 mm side length, is used as the generic antenna module feed circuit, while 150 mm long conducting rods with 5 mm diameters are used as the generic radiating elements. A cubic box with 100 mm side lengths, on which the antenna module can be located, is added into the model to simulate the effect of a 1U CubeSat platform on the radiation pattern. The simulation model includes $50\ \Omega$ ports with an identical feed power at each of the four sides of the perfectly conducting antenna module feed circuit, while the phase of each port is the negative of the corresponding position. Figure 2.6 shows the generic antenna module feed circuit, with the assigned port numbers as used in simulations and measurements. This feed circuit makes the sense of polarization right-handed towards $+z$ direction, and left-handed towards $-z$ direction.

Arm rotation angle and arm tilt angle are defined as variables for antenna arms to be rotated and tilted towards the desired direction to optimize the antenna performance.

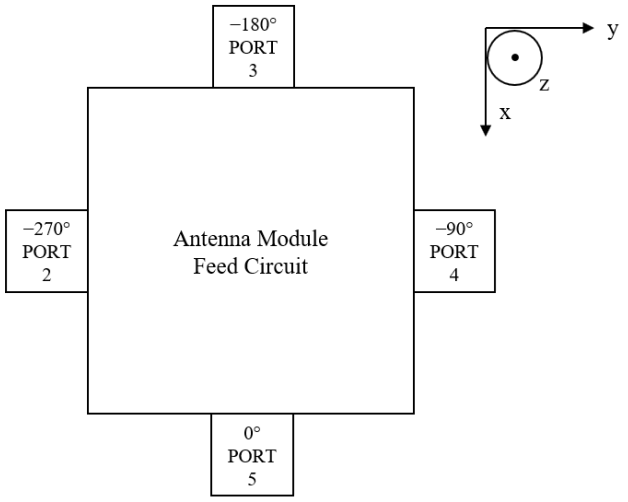

Figure 2.6: Generic antenna module feed circuit, which supports up to four arms.

The arm rotation angle variable determines the rotation angle of the tip of the each antenna arm with respect to its feed point around the z axis, whereas the arm tilt angle variable determines the angle between the axis of the antenna arm and the x-y plane.

The mechanical model of the antenna with no rotation or tilt of antenna arms is given in Figure 2.7. The gain pattern simulation result for this model is shown in Figure 2.8, which demonstrates high gain towards the poles (at $\theta = 0^\circ$ and $\theta = 180^\circ$) with opposite senses of circular polarization, as well as nulls at $\theta = 90^\circ$.

After the investigation of the initial results with no rotation or tilt, a parametric study to optimize the antenna performance is conducted in 91 steps, which includes the sweep of arm rotation angle from -90° to 90° and the sweep of arm tilt angle from 0° to 90° with 15° steps. Antenna arm lengths are kept constant in all steps of the parametric study, since tuning the arm length in small intervals to optimize the reflection coefficient, without any visible change in the radiation pattern, is a trivial task. The results of the parametric study is evaluated with respect to optimum selection criteria sets, as described in Figure 2.9. The optimum selection criteria sets involve three different objectives, i.e., optimization of the radiation in the upper hemisphere, optimization of the radiation in the lower hemisphere, and optimization of the overall pattern. The first two criteria sets aim to obtain a directive pattern, whereas the third set aims the optimization of the overall pattern, in a non-directive manner.

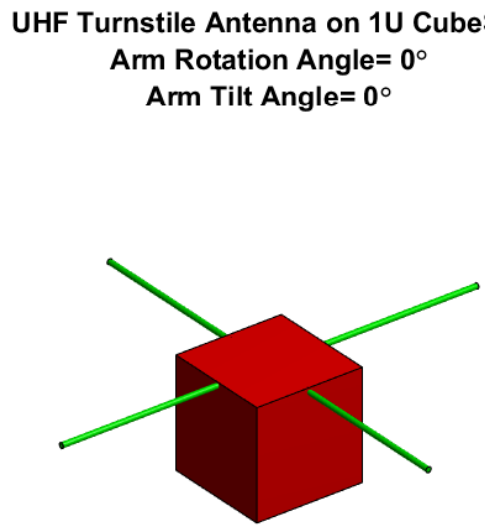

Figure 2.7: The mechanical model of the UHF turnstile antenna with no rotation or tilt of antenna arms.

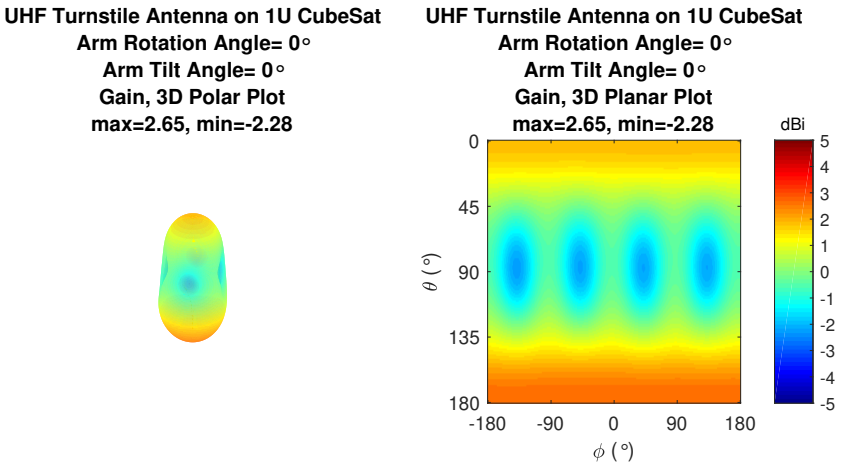

Figure 2.8: Gain of the UHF turnstile antenna with no rotation or tilt of antenna arms.

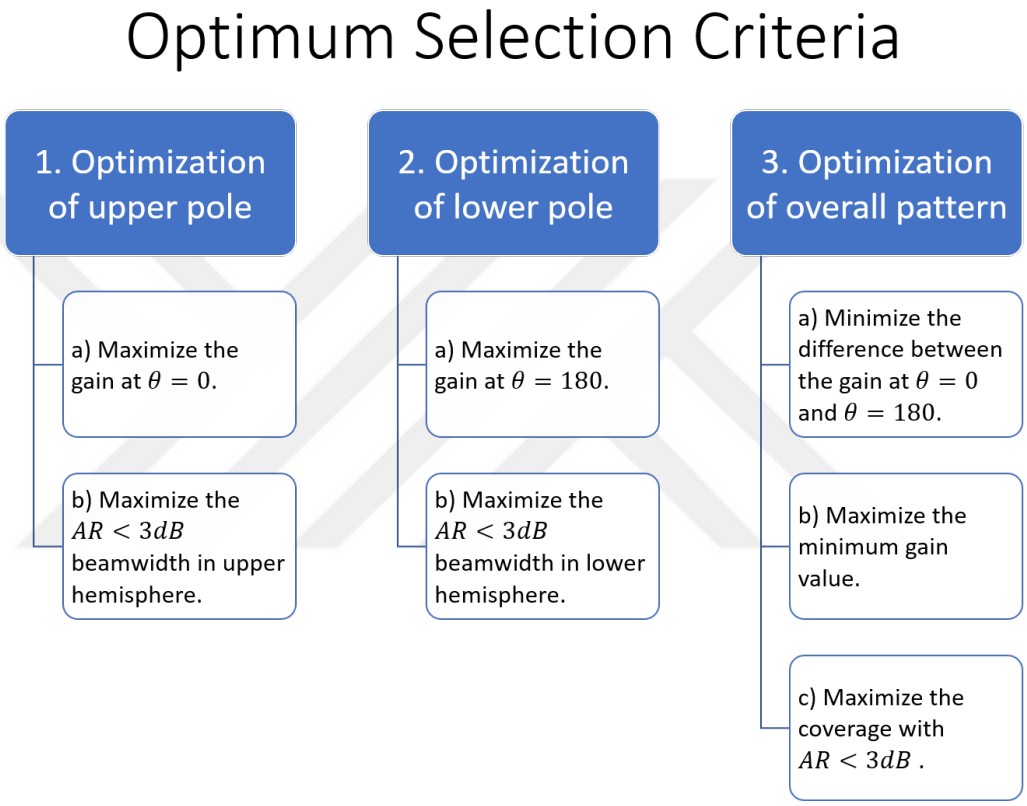

Figure 2.9: Optimum selection criteria sets to evaluate the results of the turnstile antenna parametric study.

The first criteria set, which aims to create a directive radiation pattern towards the upper pole, should provide maximum gain at $\theta = 0°$ and maximum $AR < 3$ dB beamwidth at around $\theta = 0°$. Gain values at the upper pole are plotted in Figure 2.10 for all parametric study steps. It is seen that arm rotation angle of $-45°$ and arm tilt angle of $90°$ leads to 2.456 dBi gain at $\theta = 0°$ direction, which is the maximum value among all simulation results. Likewise, as seen in Figure 2.11, maximum $AR < 3$ dB beamwidth at around $\theta = 0°$ is attained at the same configuration, as $92°$. To conclude, arm rotation angle of $-45°$ and arm tilt angle of $90°$ is found as the optimum configuration to obtain a circularly polarized directive radiation pattern towards the upper pole. The resulting mechanical model and the gain pattern simulation results are depicted in Figure 2.12 and Figure 2.13, respectively.

With the second criteria set, it is aimed to obtain a directive radiation pattern towards the lower pole, which is the opposite direction when compared to the first criteria set. Similar to the first criteria set, it is aimed to maximize the gain and the $AR < 3$ dB beamwidth, but this time at the opposite side, which is $\theta = 180°$. Gain values and $AR < 3$ dB beamwidth values at the lower pole are plotted in Figure 2.14 and Figure 2.15, respectively. It is seen that, both the maximum gain (as 3.252 dBi) and the maximum $AR < 3$ dB beamwidth (as $86°$) are obtained with arm rotation angle of $45°$ and arm tilt angle of $90°$. The obtained mechanical model and the gain pattern simulation results are presented in Figure 2.16 and Figure 2.17, respectively.

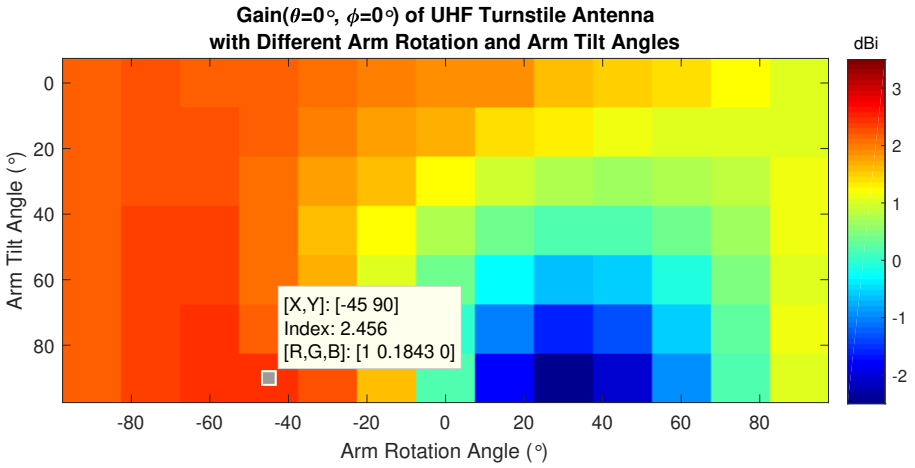

Figure 2.10: Gain of the UHF turnstile antenna at $\theta = 0°$, $\phi = 0°$ with different arm rotation and arm tilt angles.

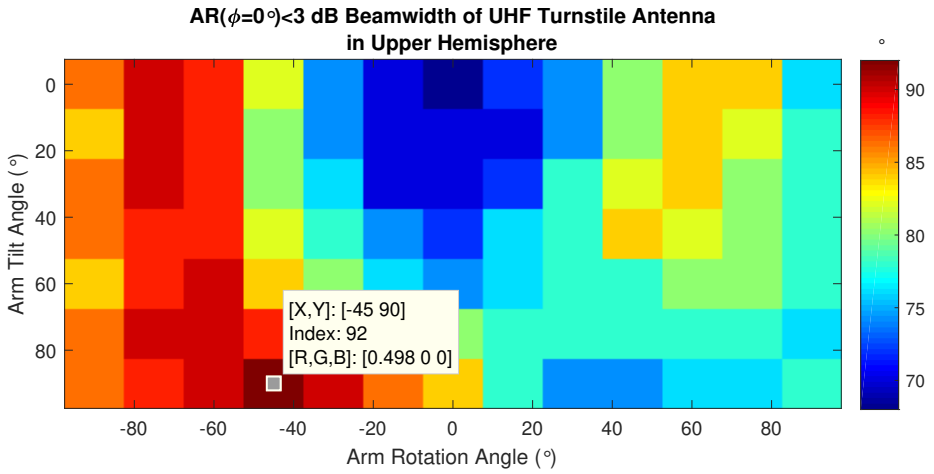

Figure 2.11: $AR < 3$ dB beamwidth of the UHF turnstile antenna at the upper hemisphere with different arm rotation and arm tilt angles.

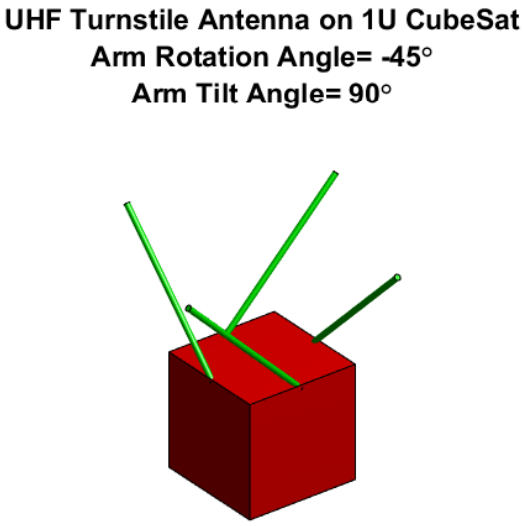

Figure 2.12: The mechanical model of the UHF turnstile antenna with -45° arm rotation angle and 90° arm tilt angle, which results in a RHCP directive radiation pattern towards $\theta = 0^{\circ}$.

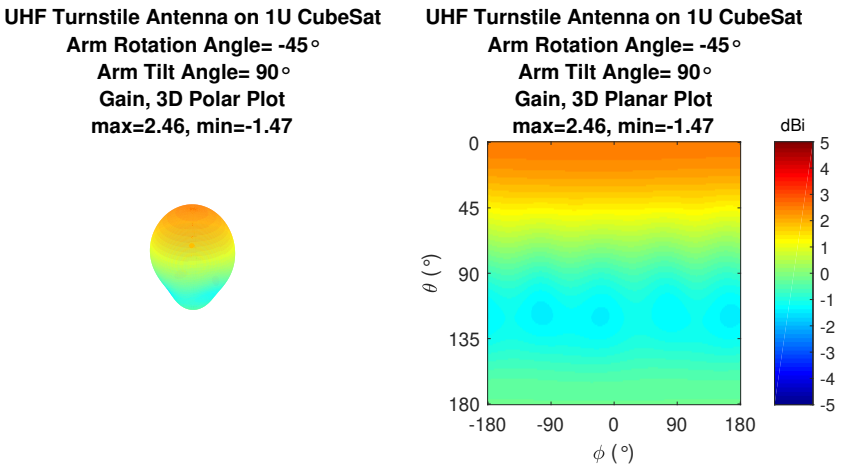

Figure 2.13: Gain of the UHF turnstile antenna with $-45°$ arm rotation angle and $90°$ arm tilt angle.

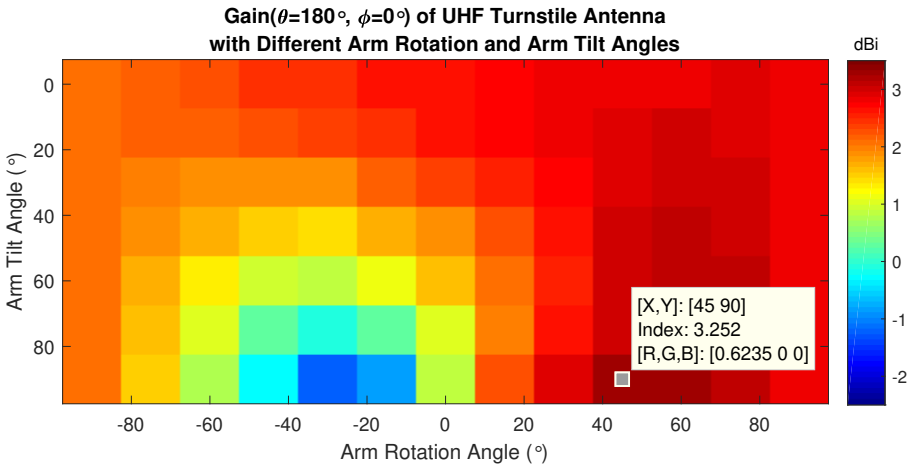

Figure 2.14: Gain of the UHF turnstile antenna at $\theta = 180°$, $\phi = 0°$ with different arm rotation and arm tilt angles.

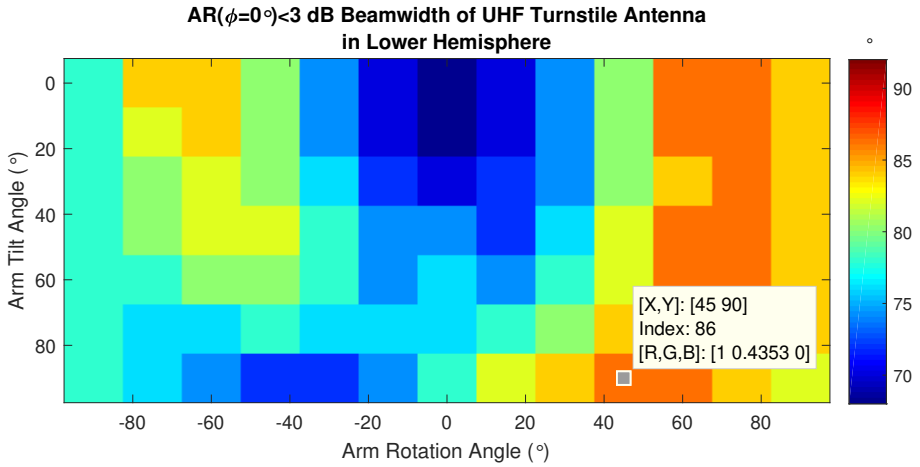

Figure 2.15: $AR < 3$ dB beamwidth of the UHF turnstile antenna at the lower hemisphere with different arm rotation and arm tilt angles.

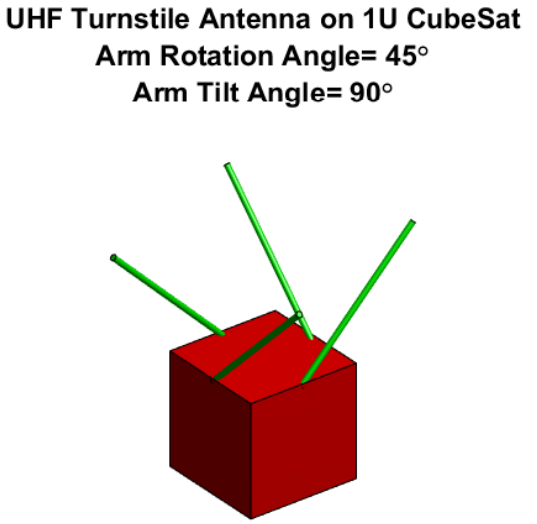

Figure 2.16: The mechanical model of the UHF turnstile antenna with $45°$ arm rotation angle and $90°$ arm tilt angle, which results in a LHCP directive radiation pattern towards $\theta = 180°$.

With the last set, which includes three criteria, the objective is to optimize the overall pattern. Optimization criterion a), which is the minimization of the difference between the gains at $\theta = 0°$ and $\theta = 180°$, aims to obtain a non-directive pattern. If the design assures that either the upper pole or the lower pole of the satellite looks towards the ground station, this optimization result can be preferred in the mission.

Values of the gain difference between $\theta = 0°$ and $\theta = 180°$ are given in Figure 2.18 for all parametric study steps. It is seen that, minimum value is obtained with arm rotation angle of $-15°$ and arm tilt angle of $60°$, as 0.045 dB. The mechanical model and the gain pattern simulation results are given in Figure 2.19 and Figure 2.20, respectively.

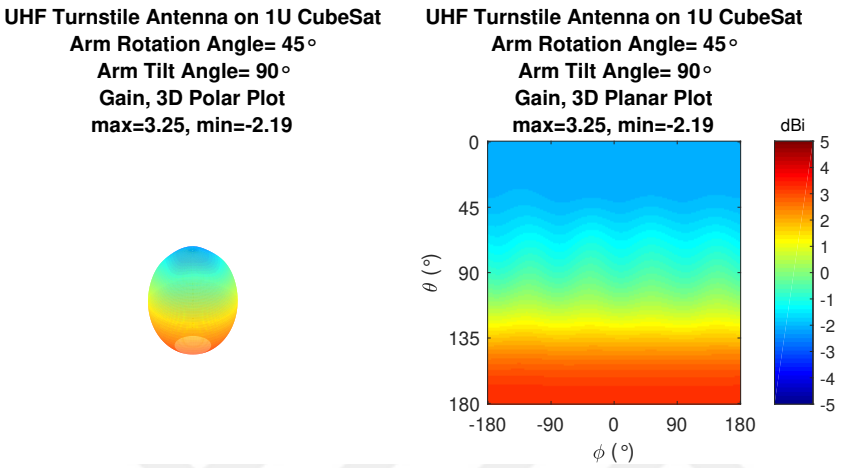

Figure 2.17: Gain of the UHF turnstile antenna with $45°$ arm rotation angle and $90°$ arm tilt angle.

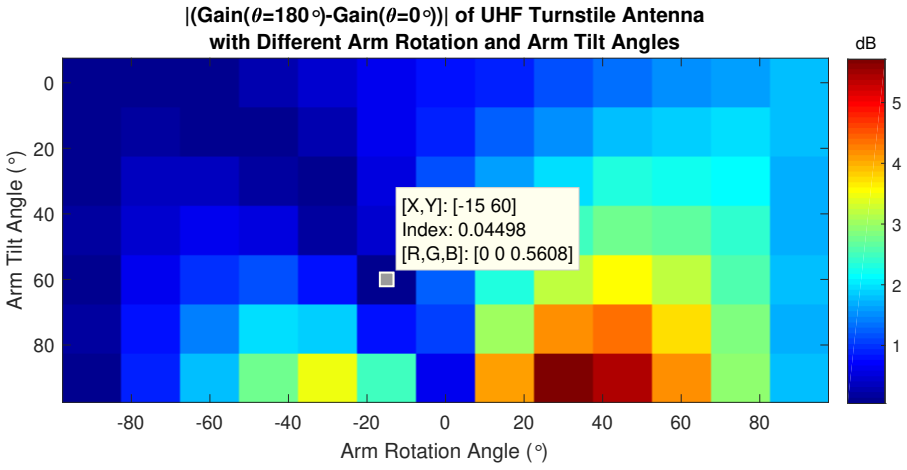

Figure 2.18: Gain difference between $\theta = 0°$ and $\theta = 180°$ of the UHF turnstile antenna with different arm rotation and arm tilt angles.

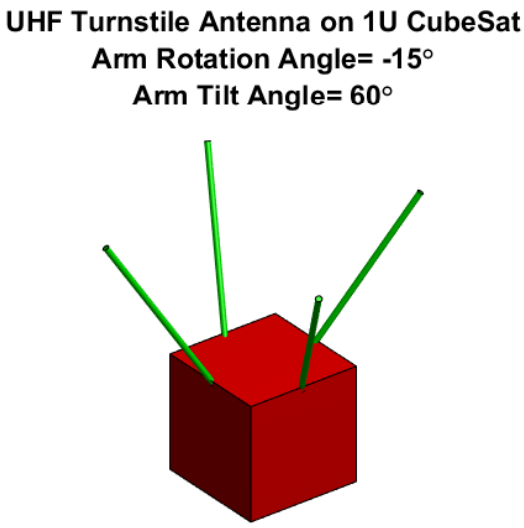

Figure 2.19: The mechanical model of the UHF turnstile antenna with $-15°$ arm rotation angle and $60°$ arm tilt angle, which results in minimum gain difference between $\theta = 0°$ and $\theta = 180°$.

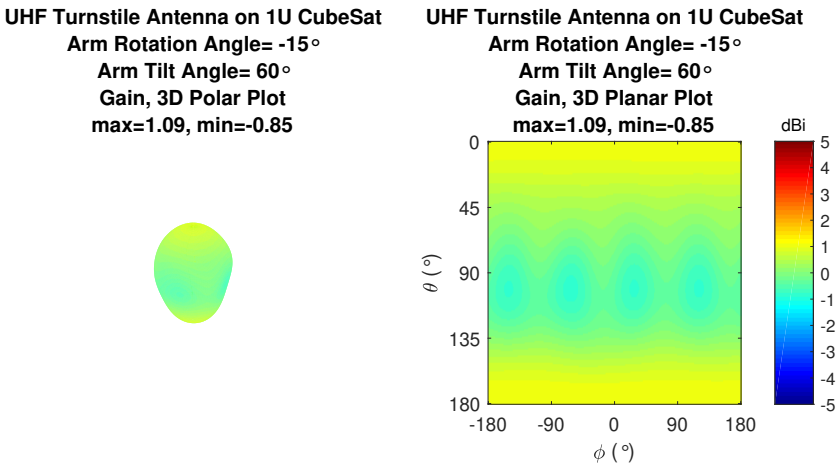

Figure 2.20: Gain of the UHF turnstile antenna with $-15°$ arm rotation angle and $60°$ arm tilt angle.

Optimization criterion b), which is the maximization of the minimum gain, aims to obtain a pattern with the lowest possibility of a link breakdown. If the design cannot assure that the side of the satellite looks towards the ground station, this optimization result can be used in the mission, for the most isotropic pattern. Minimum values of the patterns are given in Figure 2.21 for all parametric study steps. With $0°$ arm

rotation angle and 75° arm tilt angle, the minimum gain of the pattern is found as -0.37 dBi. The mechanical model and the gain pattern simulation results are given in Figure 2.22 and Figure 2.23, respectively.

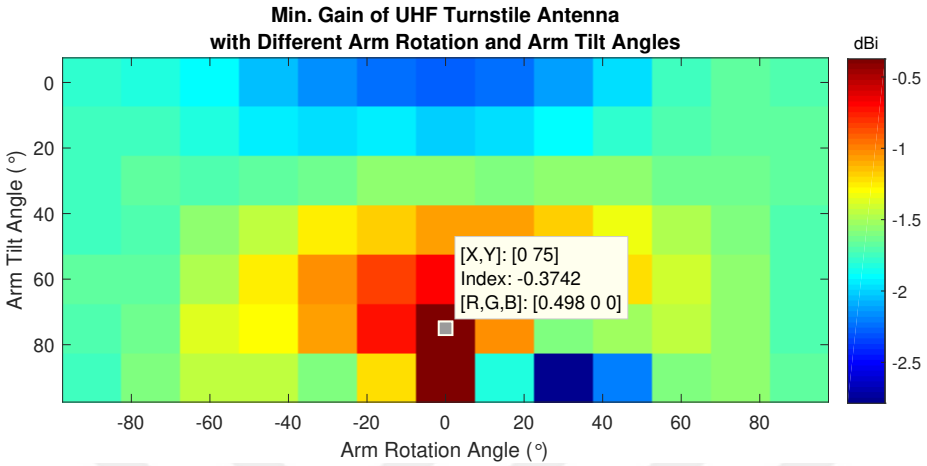

Figure 2.21: Minimum gain of the UHF turnstile antenna with different arm rotation and arm tilt angles.

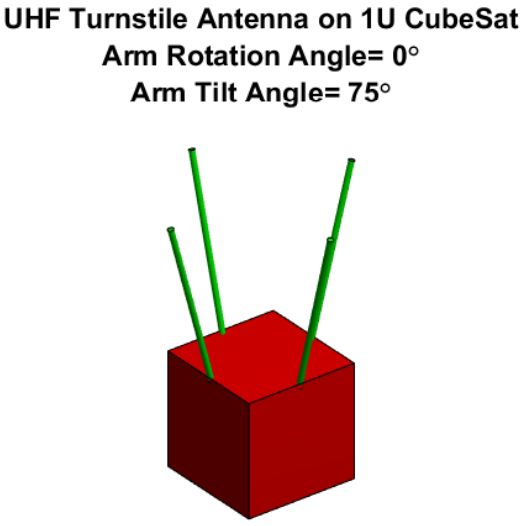

Figure 2.22: The mechanical model of the UHF turnstile antenna with 0° arm rotation angle and 75° arm tilt angle, which results in a maximized minimum gain value.

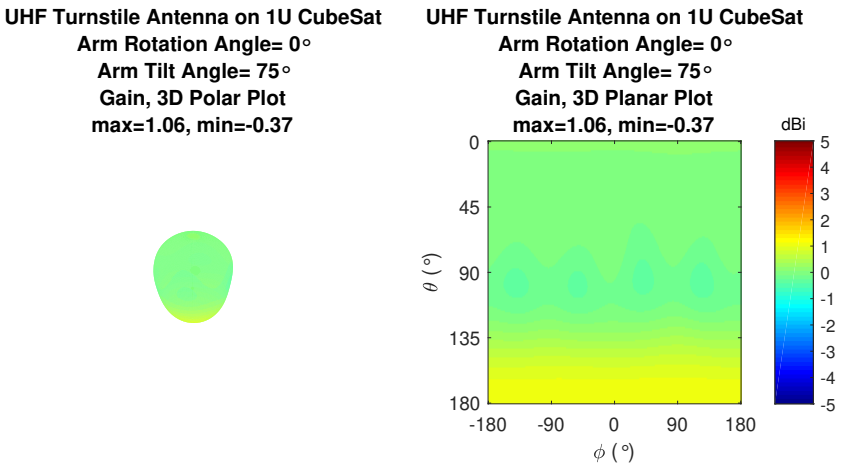

Figure 2.23: Gain of the UHF turnstile antenna with 0° arm rotation angle and 75° arm tilt angle.

Optimization criterion c), which is the last among the set, aims to maximize the radiation area with circular polarization. The percentage of the areas with $AR < 3$ dB is given in Figure 2.24 for all parametric study steps. It is seen that, different rotation and tilt angles of the arms result in similar values, making this optimization practically less important.

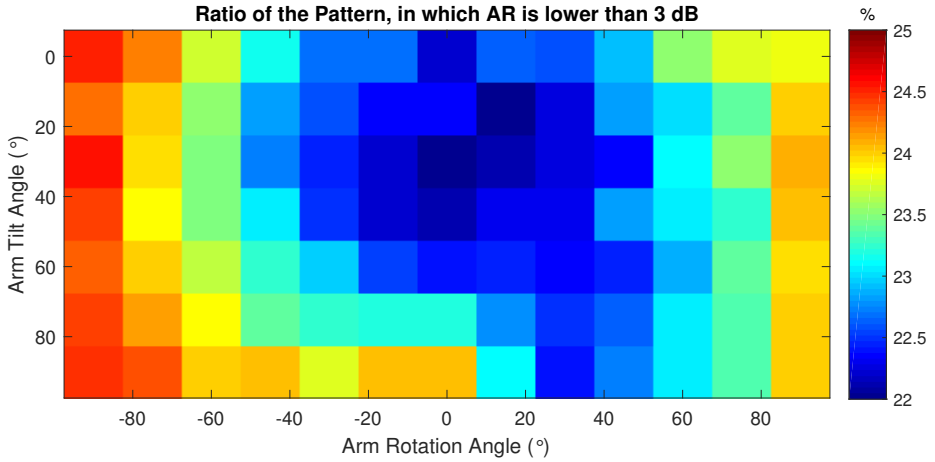

Figure 2.24: Percentage of the radiation areas with $AR < 3$ dB for the UHF turnstile antenna with different arm rotation and arm tilt angles.

2.2.3 Design and Simulation of Feed Circuit

In order to feed the turnstile antenna arms by successive 90° phase differences between them, a four-way quadrature splitter is needed, as shown in Figure 2.6. For this purpose, a passive feeding circuit is designed and simulated in NI AWR design and simulation environment. The design is started with ideal blocks and continued with component selection. Then, the selected components are inserted into the simulation model, using the S-parameter files provided by the suppliers. Layout design and fine tuning are conducted before the fabrication of the circuit. Design of the four-way quadrature splitter with ideal blocks is given in Figure 2.25. By using a balun transformer, the input signal is divided into two equal parts with opposite phases. Then, quadrature hybrids are used for an equal division with phase quadrature. The resulting structure divides the input power into four equal parts, with 90° phase differences, as desired.

After the initial simulations with ideal blocks, appropriate components are selected and inserted into the design. Real components have finite insertion losses, as well as phase and amplitude unbalances, when compared to lossless and perfectly phased ideal components. Among the available components in the market, the balun transformer ADT2-1T-1P+ and the quadrature hybrid QCN-3+ from Mini Circuits are selected due to their high performance and availability. Components are connected to each other with coplanar waveguides, which have 0.33 mm widths and 0.3 mm spacings to the coplanar ground on the FR4 material with 0.2 mm thickness. Phase unbalances between the components are compensated by using different trace lengths. Simulations are started at schematic level, while final tuning is made with EM simulations. The recommended layouts for the components are prepared in the simulation environment, and S-parameter files are inserted. The prepared layout for EM simulations, which is a square board with 100 mm side lengths, is given in Figure 2.26. The input port for radio connection is planned as a through hole SMA connector at the middle, whereas the output ports for antenna arm connections are planned as edge-mount SMA connectors at the edges of the PCB.

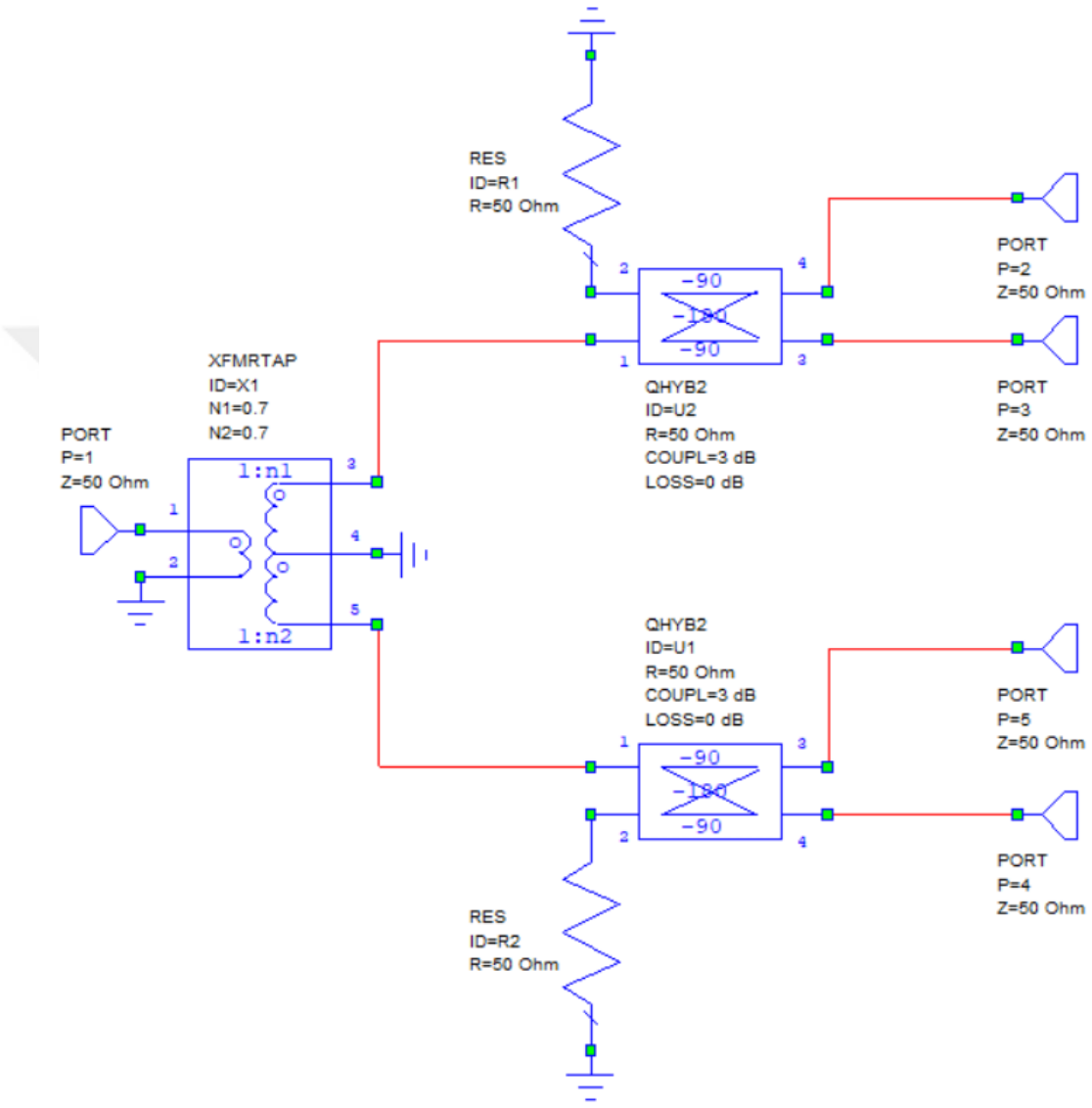

Figure 2.25: Design of the four-way quadrature splitter with ideal blocks.

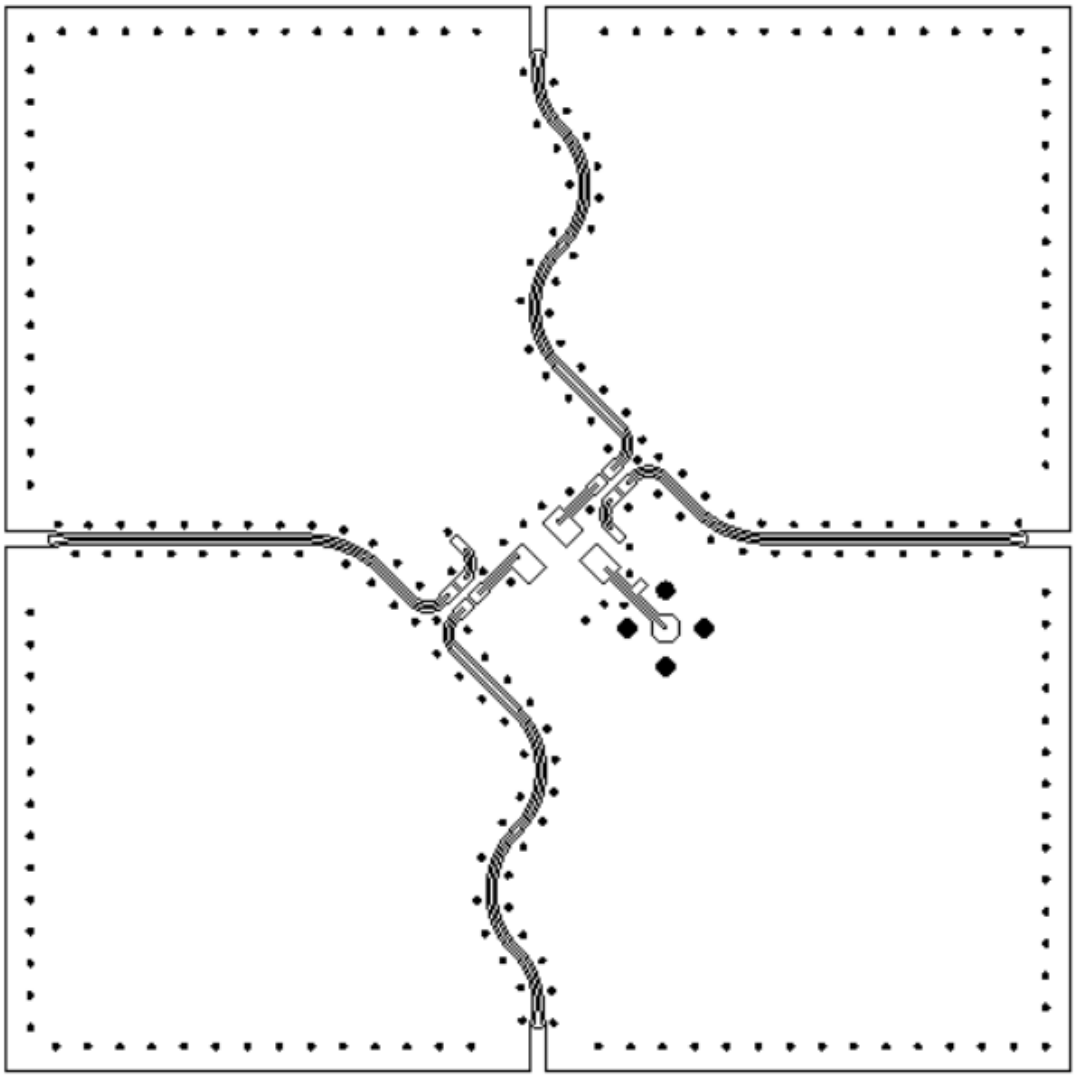

Figure 2.26: EM simulation layout of the UHF turnstile antenna feed circuit.

EM simulation results for the antenna feed circuit is given in Figure 2.27. It is seen that phase differences between the output ports are obtained as $90 \pm 1^{\circ}$ by the optimization of the trace lengths, while minimum and maximum transfer magnitudes are found as -7.76 dB and -7.23 dB, respectively. This means that the insertion loss of the antenna feed circuit is approximately 1.5 dB and the maximum magnitude unbalance is approximately 0.5 dB due to the insertion loss and unbalance of the selected components.

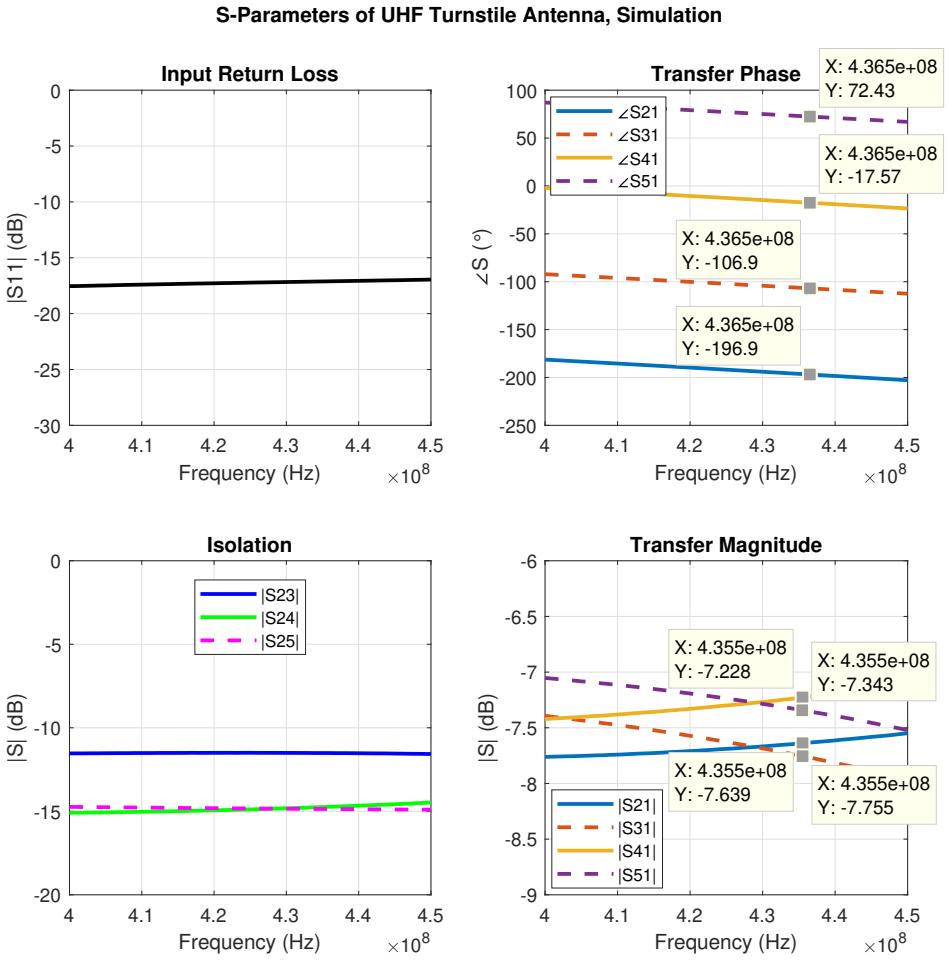

Figure 2.27: EM simulation results of the UHF turnstile antenna feed circuit.

2.2.4 Fabrication and Measurement

The designed and optimized feed circuit is tailored for fabrication, by adding drill holes, soldermask, and silkscreen layers onto the layout used for simulation. Because of the fragility of the board (with 0.2 mm thickness) used in the design, a four-layer stackup (JLC7628) is used instead of a single dielectric layer. Fabricated and assembled antenna feed circuit is given in Figure 2.28. The S-parameter measurement results, which comply with the simulation results, are given in Figure 2.29. The phase differences between the output ports are measured as $90 \pm 2.5°$. In addition, minimum and maximum transfer magnitudes are found as -8.24 dB and -6.64 dB, respectively. The average insertion loss at the ports is 1.5 dB, as in the simulation results. The maximum magnitude unbalance between the output ports is approximately 1.5 dB due to the different performances of the components provided by the supplier, in comparison to their datasheets.

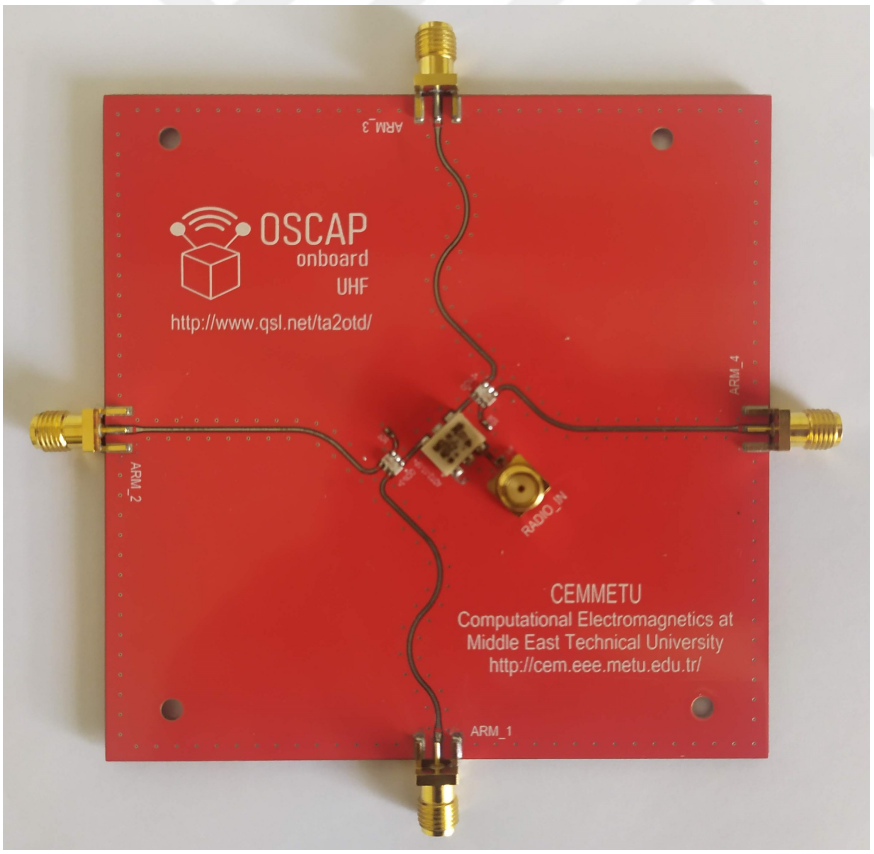

Figure 2.28: Fabricated and assembled antenna feed circuit.

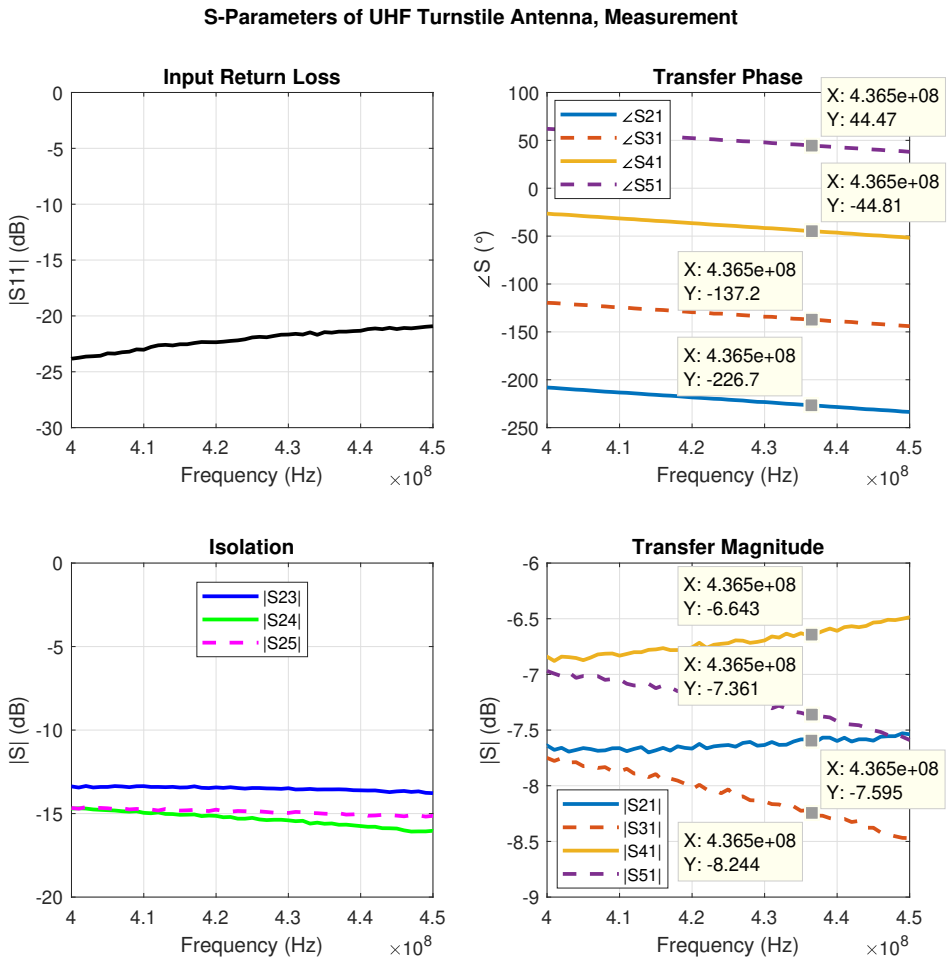

Figure 2.29: Measurement results of the UHF turnstile antenna feed circuit.

After the S-parameter measurements, the arms of the antenna are mounted onto the feed circuit. Telescopic antenna elements with hinges, which enable different orientation angles, are used for easy prototyping. Arm rotation angle of $-45°$ and arm tilt angle of $90°$ are used, to create an RHCP pattern towards $\theta = 0°$. A CubeSat chassis of size 1U made of aluminum is used as the platform. Also, laser-cut plexiglass interface pieces are placed together with an absorber, to mount the antenna onto the measurement setup. The overall prototype placed in the anechoic chamber is shown in Figure 2.30.

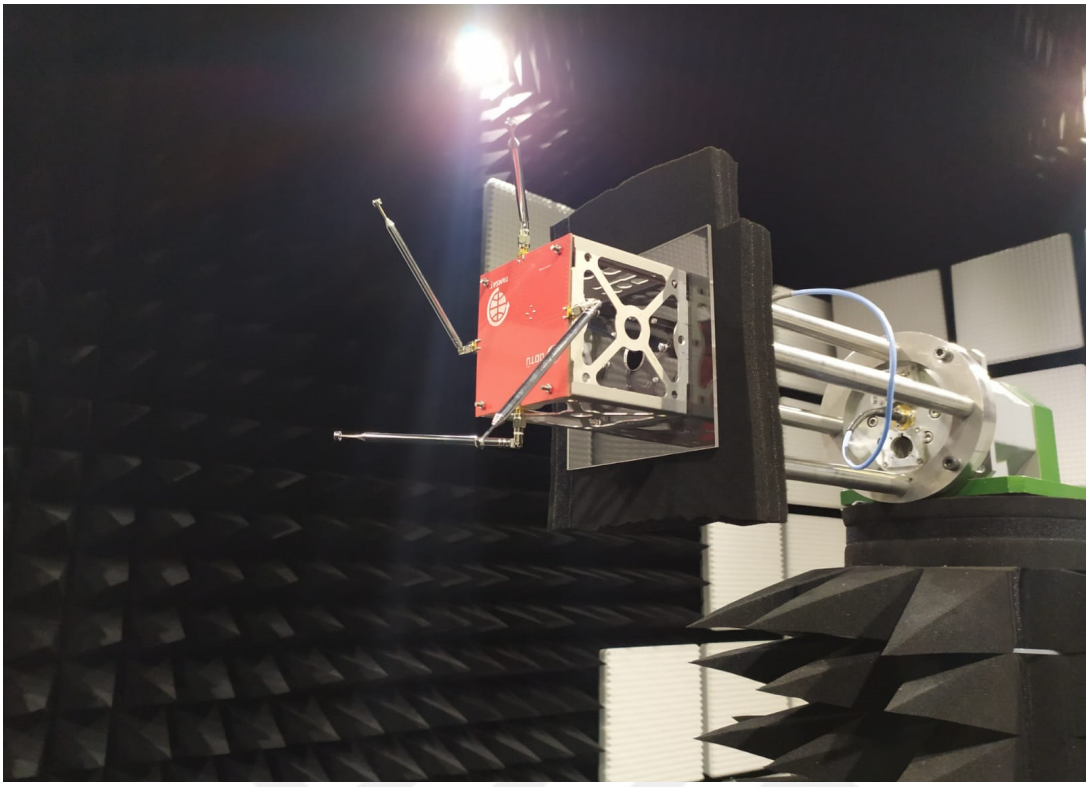

Figure 2.30: The antenna prototype placed in the anechoic chamber.

Considering the first results, telescopic antenna elements with hinges are observed to have high reflection coefficient values, even when their lengths are tuned. This leads to linear polarization, instead of the desired circular polarization. To have better reflection coefficient performances, telescopic antenna elements are replaced by plastic-covered monopole antennas operating in the ISM band. Due to the absence of a ground surface, poor reflection coefficient of the monopole antenna elements at around -2 dB are tuned with aluminum tape, as shown in Figure 2.31. Reflection coefficients are enhanced to -13 dB by this simple yet effective tuning process.

Radiation pattern measurements after tuning lead to successful results with RHCP radiation, as given in Figure 2.32, together with the simulation result. In the measurement result, the asymmetric pattern and the back lobe are due to reflections from the walls, which have absorbers designed for the frequencies higher than 1 GHz. Normalized gain result with a rotating linearly polarized measurement antenna is given in Figure 2.33. It is seen that axial ratio of the antenna at the boresight direction is approximately 1.1 dB.

Figure 2.31: Monopole antenna tuning with aluminum tape.

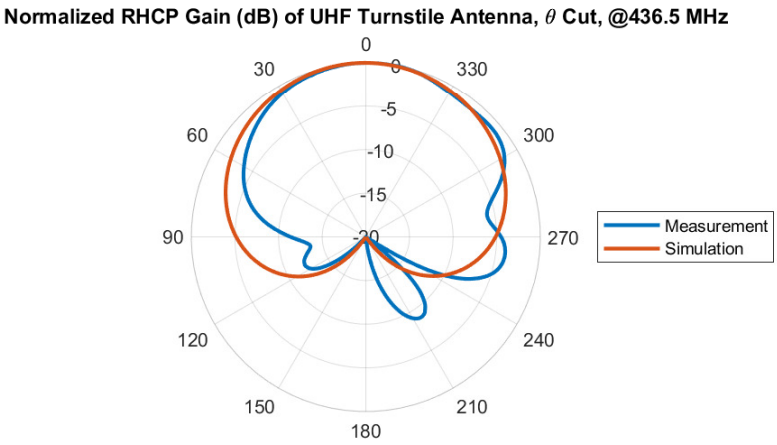

Figure 2.32: Measurement and simulation results for the radiation pattern.

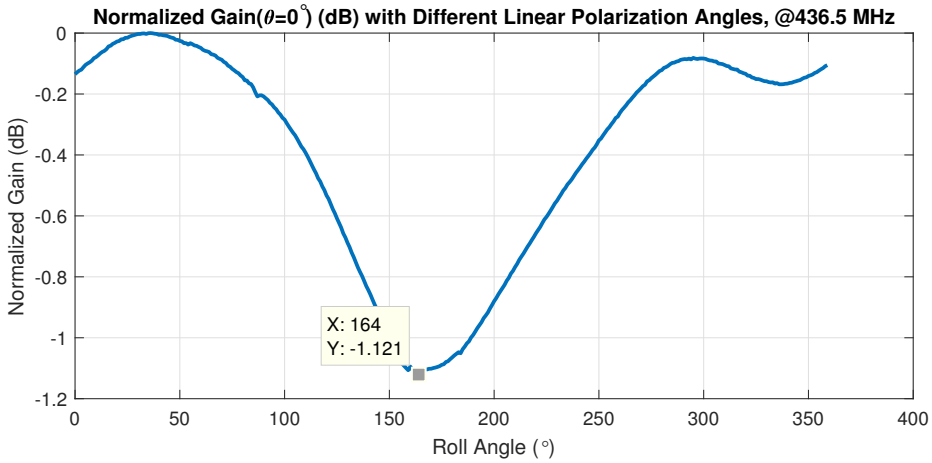

Figure 2.33: Normalized gain obtained with different polarization directions of the linearly polarized measurement antenna.

2.3 V/UHF Circularly Polarized On-Board Antenna Configuration: Dual-band Trapped Turnstile Antenna

In this section, a multi-frequency variant of the on-board turnstile antenna, i.e., a novel dual-band trapped V/UHF turnstile antenna, is presented. This design aims to ease the mechanical deployment process and decrease the mass of the CubeSat, thanks to the unification of operations at two frequencies in a single antenna module. In the proposed configuration, VHF and UHF operations are maintained from the same port. The feed circuit is planned to be implemented as in the UHF case, but this time with components opearating not only in the UHF band, but also in the VHF band. The antenna arms are trapped by inserting parallel LC sections at the selected positions to match the antenna impedance to the port impedance at both frequencies. Theoretical information on antenna traps and design of a V/UHF trapped dipole antenna are given in next subsection, followed by the design and simulation results for the novel dual-band trapped V/UHF turnstile antenna.

2.3.1 Background on Antenna Trapping and Design of a V/UHF Trapped Dipole Antenna

Antenna trapping technique is mostly used in sub-GHz frequency bands, especially for wire antennas, to obtain multi-frequency operation. The idea of antenna trapping is to insert a band-stop filter involving a parallel LC circuit, which acts like an infinitely large impedance termination at the resonant frequency of the trap, to prevent current flow from the trap position towards the tip of the antenna. This way, the length of the antenna is shortened and the antenna impedance is matched at the resonant frequency [37]. At the other frequencies, the trap acts like a short circuit, as desired. A dual-band trapped monopole antenna is shown in Figure 2.34 [38].

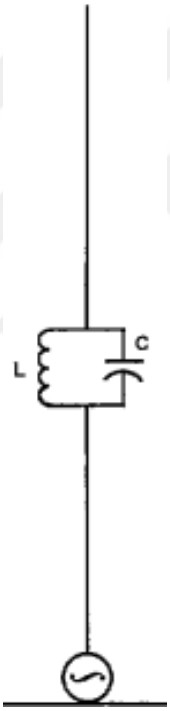

Figure 2.34: Trapped monopole antenna [38].

The resonant frequency of a trap, which is a parallel LC circuit, is calculated as

$$f_{LC\ Trap} = \frac{1}{\sqrt{LC}} \frac{1}{2\pi} \tag{2.1}$$

assuming that the inductor and capacitor are ideal. The impedance of the trap circuit

by taking into account the finite series resistance of the inductor is calculated as

$$Z_{LC\ Trap} = \left[\frac{1}{j2\pi fL + R}\, j2\pi fC \right]^{-1}. \tag{2.2}$$

A simple trapped dual-band V/UHF dipole antenna is simulated in 4NEC2 simulation environment to test the antenna trapping concept. The antenna model in the environment is depicted in Figure 2.35. Blue squares show trap positions, which make antenna resonate at the resonant frequency of 436.5 MHz, in addition to the full length resonance of 145.5 MHz.

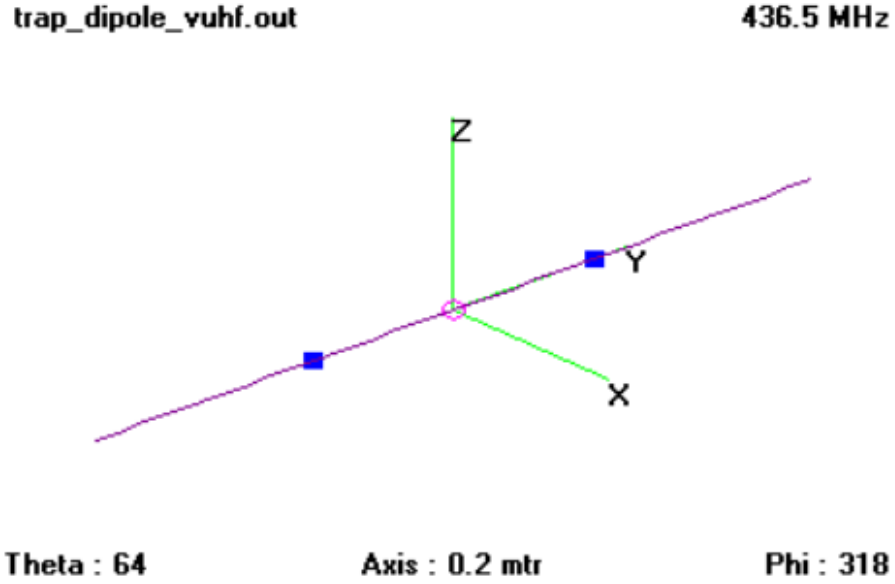

Figure 2.35: Trapped dipole antenna modeled in 4NEC2.

By using Equation 2.1, L and C values of the trap are selected for the resonant frequency of 436.5 MHz. A finite quality factor of 55 is used for the inductor and impedance is calculated by using Equation 2.2 via fine tuning of L and C values, to finalize the design. Figure 2.36 shows the real and imaginary parts of the impedance of the designed trap, using $L = 102$ nH and $C = 1.3$ pF. Reflection coefficient simulation result for the model in 4NEC2 is shown in Figure 2.37. It is seen that the antenna is successfully matched at 145.5 MHz and 436.5 MHz. Simulation results for antenna pattern at 145.5 MHz and 436.5 MHz are further given in Figure 2.38. The patterns are similar to each other, being omnidirectional with half-wave dipole characteristics.

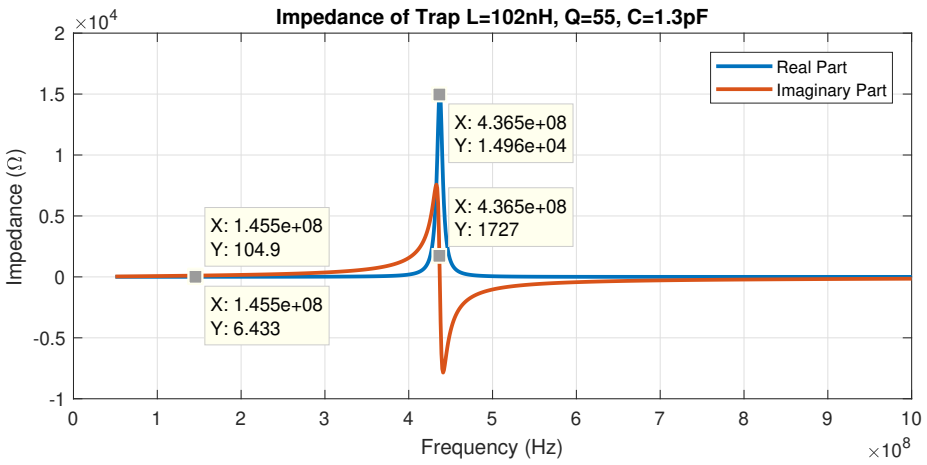

Figure 2.36: Impedance values of the designed trap at different frequencies.

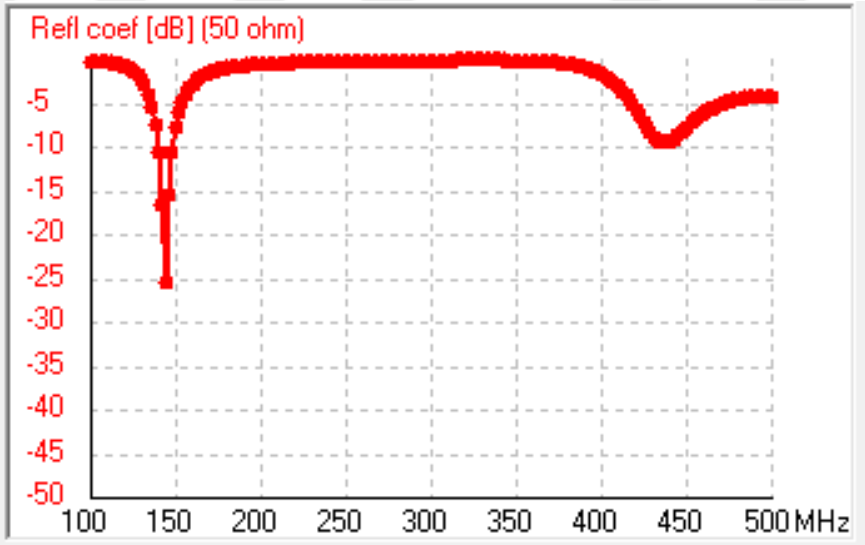

Figure 2.37: Reflection coefficient simulation result for the trapped dipole antenna in 4NEC2.

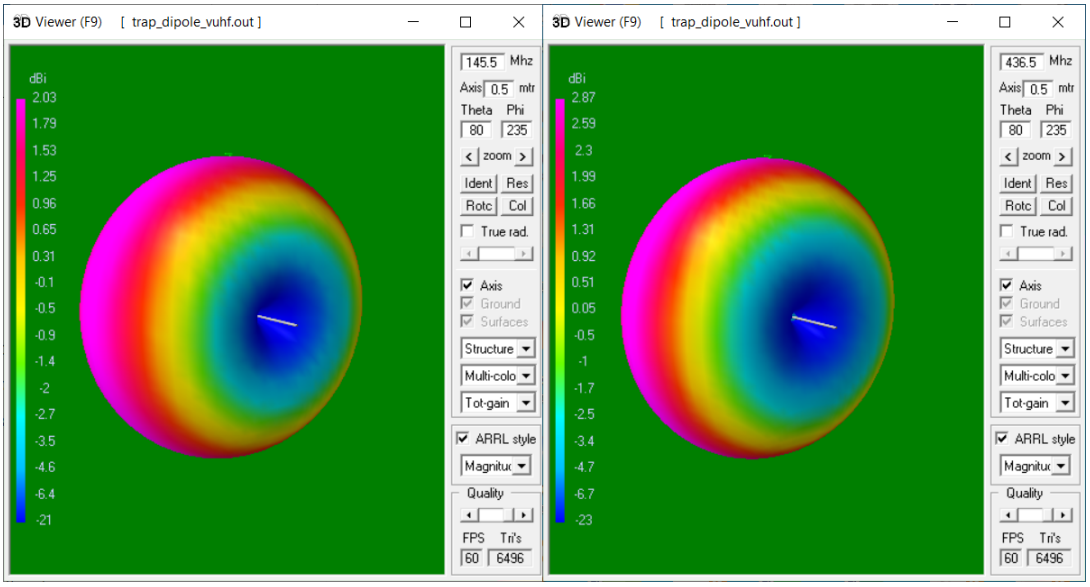

Figure 2.38: Radiation pattern simulation results for the trapped dipole antenna in 4NEC2 at 145.5 MHz (left) and 436.5 MHz (right).

2.3.2 Design of Dual-Band Trapped V/UHF Turnstile Antenna

Dual-band version of the turnstile antenna is simulated in ANSYS Electronics Desktop simulation environment, using the initial results obtained by the trapped dipole antenna simulations in 4NEC2. The trap capacitance is tuned by changing the capacitance value to 0.8 pF. The position of the trap is tuned for a radiation pattern similar to the one obtained for the single frequency design. Specifically, the trap position is selected as 200 mm whereas the full antenna length is selected as 410 mm. Reflection coefficient for an antenna arm without any rotation or tilt is given in Figure 2.39, where successful match is observed at both operation frequencies.

The gain patterns (again without any rotation or tilt) at 145.5 MHz and 436.5 MHz are presented in Figure 2.40 and Figure 2.41, respectively. Due to the larger electrical size of the 1U chassis at the higher frequencies, the gain pattern is asymmetric in the UHF band, whereas there is no significant effect of the chassis in the VHF band.

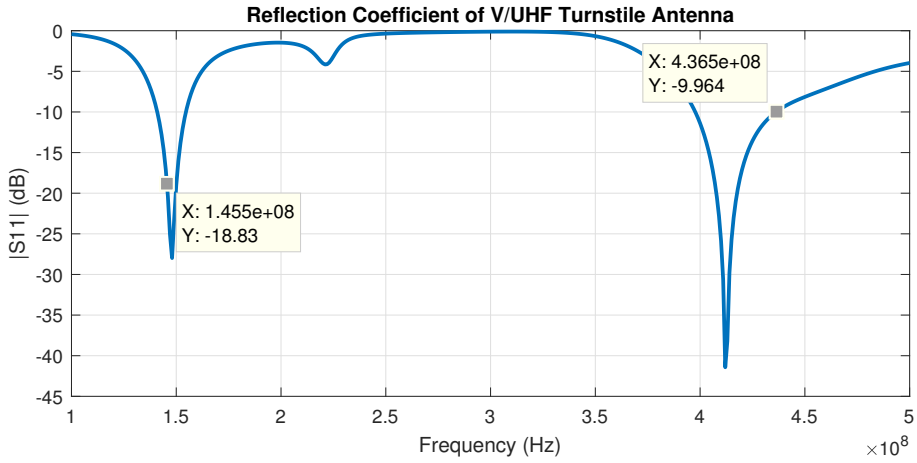

Figure 2.39: Reflection coefficient result for an antenna arm of the V/UHF turnstile antenna without any rotation or tilt.

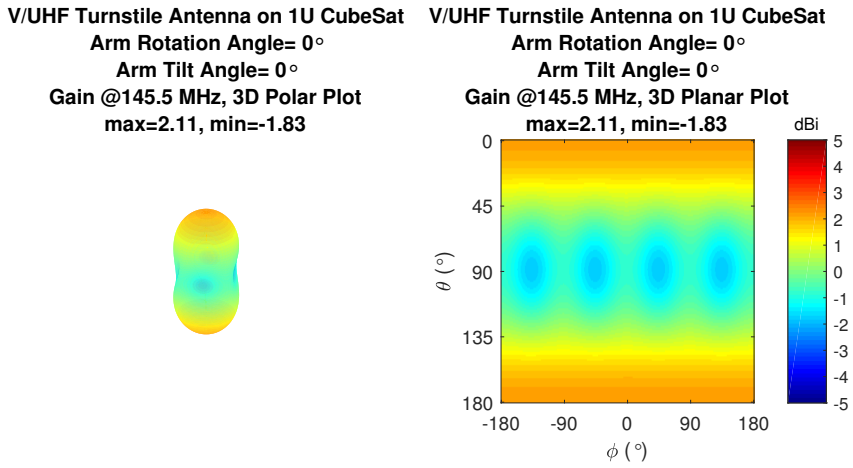

Figure 2.40: Gain of the V/UHF turnstile antenna without any rotation or tilt at 145.5 MHz.

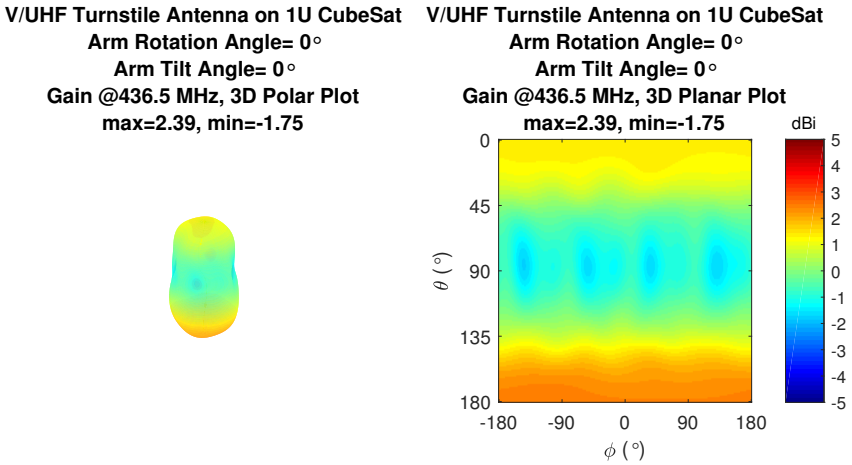

Figure 2.41: Gain of the V/UHF turnstile antenna without any rotation or tilt at 436.5 MHz.

CHAPTER 3

GROUND STATION ANTENNA SYSTEMS

Ground stations are the earth segments of aerospace missions. Aerospace platforms, including all types of aircrafts, satellites, missiles, and radiosondes are linked to the Earth by means of ground stations. The missions might include stationary or moving platforms with respect to ground stations.

The block diagram of a simple ground station system is given in Figure 3.1. In the block diagram, it is assumed that the transceiver is a single-port radio with low output power, while a single antenna is used for both trasmit and receive operations. To communicate with the platform, there are two modes to be selected: receiver (RX) mode with a low-noise amplifier (LNA) and transmitter (TX) mode with a power amplifier (PA). This structure is also implemented in ICs for low power, short range systems, as in the example of [39].

In the TX mode, the data from the ground station is sent to the platform with high RF output power via the PA. The output power of the PA changes from several watts to several hundreds of watts, sometimes being even in the order of kilowatts, according to the link budget calculations [40]. In the RX mode, the data sent from the platform is received by the LNA, which is placed close to the antenna to have the maximum possible sensitivity in the RX mode [41]. Switches with isolation values high enough to protect the LNA from high RF power levels should be used in this type of applications. The RF switch controller, which sets the states of the switches, is a device with logic output pins. Sometimes it is named as “sequencer”, which sets the time sequence of switch states by inserting the required time delays in between [42]. The antenna rotator directs the antenna to the desired azimuth and elevation angles. The ground station computer is the subsystem, in which all other subsystems and their

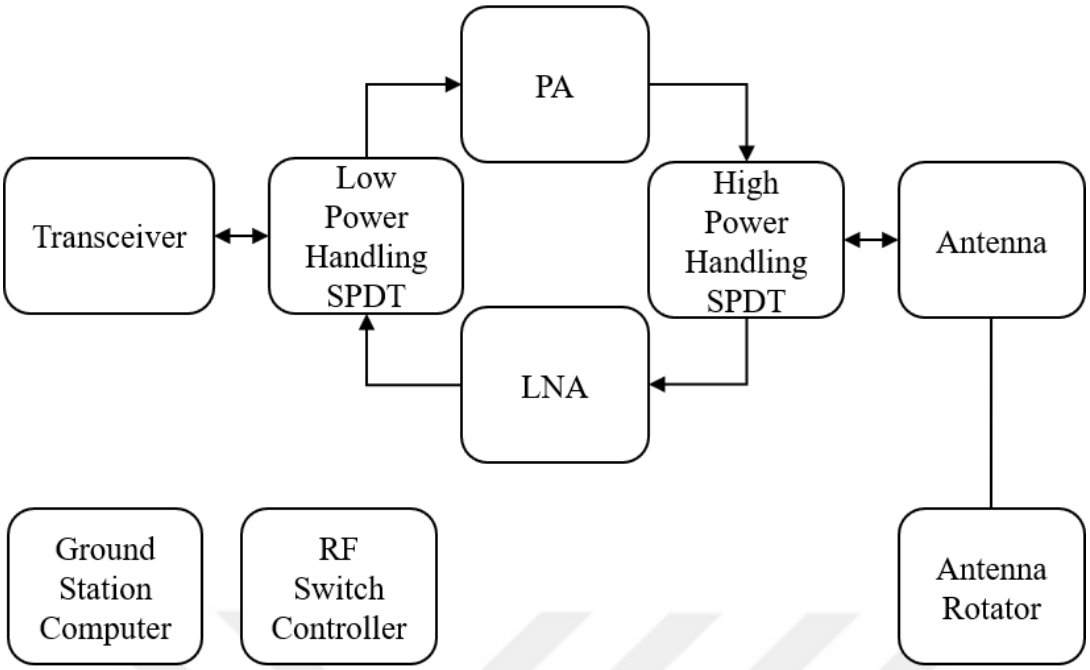

Figure 3.1: A simple ground station system (SPDT: Single-pole, double-throw switch).

parameters are controlled, including the azimuth and elevation angles of the antenna rotator, doppler frequency shift compensation of the transceiver, and the states of the RF switch controller.

Mission requirements determine the structure of a ground station. For example, in meteorological missions, an RX-only ground station is used to receive the downlink meteorological measurement data obtained by a radiosonde [43]. Whereas in CubeSat missions that include an FM radio repeater, the uplink voice data transmitted by a ground station is repeated as downlink with a different frequency to other ground stations [44]. Ground stations for geostationary satellites do not require antenna rotators, because of the stationary positions of the platforms with respect to the ground stations. Sometimes, ground stations are placed at different locations and used collaboratively as a network to receive the signal of a platform as it orbits [45].

The study presented in this chapter is focused on antenna systems for ground stations. First, possible antenna types and selection criteria are presented. Then, design and realization of a circularly polarized VHF Yagi antenna are reported. Finally, a circularly polarized UHF Yagi antenna design is presented.

3.1 Antenna Types and Selection Criteria

The antennas that can used in a ground station are selected regarding several factors, such as operating frequency, polarization, and gain.

Frequency of operation for a system depends on the bandwidth requirement of the communication operation. The frequency spectrum is strictly controlled by regulatory authorities. For example, amateur LEO satellite missions mostly use the lower end of the satellite frequency spectrum, which are VHF and UHF ham radio bands for low data rate operations [46]. Similarly, meteorological radisonde systems use frequencies in the lower UHF band [47]. It is possible to use simple wire antennas and antenna arrays in these frequency bands. On the other hand, S-Band is the new trend for higher bandwidth requirements in amateur aerospace missions; this frequency band is the spectrum portion that also includes Wi-Fi devices. It is possible to use patch arrays in this band. High data rate military and civilian systems use higher frequency sub-bands with SHF classification. Generally, reflector antennas are used in these higher frequency bands to get high directivity [48].

When the polarization of the on-board antenna of a CubeSat platform is not aligned with the polarization of the ground station antenna, polarization losses inevitably occur, leading to a degradation on the link performance. To minimize the degradation, it is desired to use circularly polarized antennas in ground stations, whenever possible. In addition to the alignment problem, the Faraday rotation phenomenon is an important issue to take into account when the platform is outside the atmosphere. Specifically, due to the Faraday rotation, right-handed and left-handed waves propagating through ionosphere have different phase velocities, which causes a change in the rotation angle of the polarization vector [49]. Then, a switchable polarization antenna or two separate antennas with different senses of circular polarization should be used to maximize the performance of the link between the platform and ground.

The physical size is certainly an important aspect when designing ground station antenna. Because of the difficulty in the fabrication of large structures and the high cost of rotators to be used for them, generally the size, so the directivity, is often limited by allocated economical resources.

If the margin in the link budget calculation is enough for operation with low gain, it is advantageous to use non-directive antennas in the ground station considering the cost, by eliminating large directive antennas and costly rotators. The inevitable result of this selection is relatively poor performance when compared to ground stations with directive antennas. The first disadvantage of using non-directive antennas is receiving unintended signals from the environment. Second, due to the low gain towards the platform, higher output power is required for a successful uplink operation. Hence, non-directive antenna types are generally not preferred for uplink operations, while they are still preferred in low-cost receive station setups and emergency backups to complement directive antennas as secondary. Such a secondary antenna is planned for the case of a rotator fault or a direction detection failure. Using a non-directive antenna at high frequencies, such as in S-Band and X-Band, is not generally possible, due to the requirement of high directivity to compensate excessive propagation losses, as indicated by Friis formula [50].

A summary of the most common types of directive and non-directive antennas for ground station setups are given in [51]. Monopole, dipole, turnstile, cross-dipole, V-dipole, egg-beater, and normal mode helix structures are the most common types of non-directive antennas, whereas Yagi-Uda, log-periodic, and patch arrays, as well as reflectors with different types of feeds are the most common types of directive antennas.

3.2 Design and Fabrication of a Directive Antenna: Circularly Polarized VHF Yagi Antenna

A circularly polarized VHF Yagi antenna is designed and constructed in the scope of this thesis. The selection of this antenna type is due to its high performance, despite of its relatively simple structure. The design process is started with theoretical design and continued with simulations. The designed structure is fabricated by a team of amateur radio enthusiasts using aluminum rods and home-brew PCB fabrication techniques. An antenna in the UHF band is also designed and prepared for fabrication after acquiring experience from the VHF antenna. This section is divided into subtitles to explain the details of the work step by step.

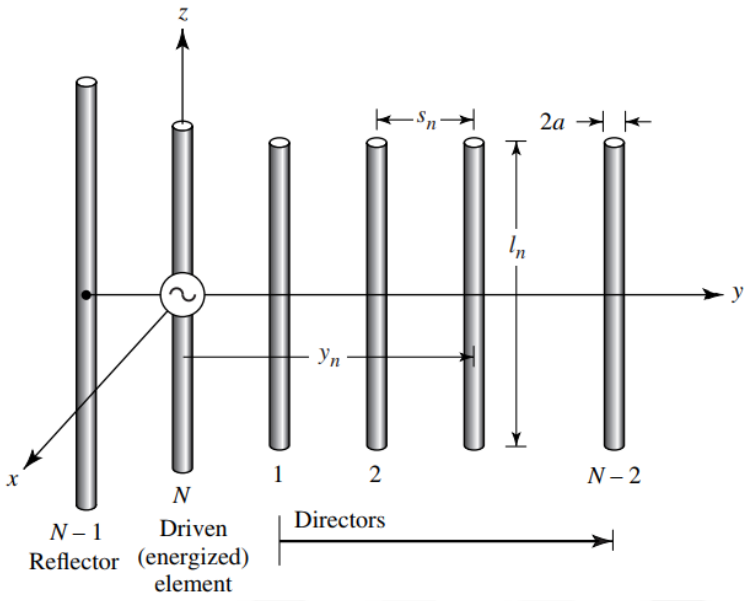

Figure 3.2: Yagi antenna with N elements [53].

3.2.1 Background on Yagi Antenna

The invention of Yagi-Uda antennas is one of the milestones in antenna engineering; they are invented by Hidetsugu Yagi and Shintaro Uda of Tohoku Imperial University, Japan, in 1920s. They are mostly named as Yagi antennas in short.

As described in [52], when a rod of length equal to or slightly longer than half of the wavelength is placed near a radiating source, it acts as a reflector. In contrast, when a rod of length slightly shorter than half of the wavelength is placed near a radiating source, it acts as a director. By placing passive linear rods as reflectors and directors near a radiating dipole to create constructive interference in the desired direction of forward propagation and destructive interference in the desired direction of backward propagation, a Yagi antenna can be constructed. The importance of Yagi antennas come from the fact that they offer high levels of gain with relatively simple geometries having low weights and high wind resistances. Unsurprisingly, they have been the most widespread antennas by far, as they are preferred to receive TV signals in terrestrial broadcasts. A description of a Yagi antenna with N elements can be seen in Figure 3.2.

In a Yagi antenna, the lengths of the elements are around half of the wavelength, while

spacings between them are around one-fifth of the wavelength, in general. Optimization of element lengths and spacings is relatively easy by using numerical tools. However, because of the popularity and widespread use of Yagi antennas, several design reports are published to ease the process by providing optimized design parameters. Reference [53] includes a design procedure that starts by the parameters published in [54] and continues with optimization for minor changes. Optimization is required mainly due to the effect of the finite-diameter metallic boom that carries the elements. A list of optimized design parameters from [54] is given in Table 3.1.

Table 3.1: Optimized design parameters for Yagi arrays to achieve different gain values [54].

Optimized Lengths of Yagi Antennas for Six Different Lengths							
Length of Yagi, λ		0.4	0.8	1.2	2.2	3.2	4.2
Length of Reflector, λ		0.482	0.482	0.482	0.482	0.482	0.475
Length of Director, λ	1st	0.424	0.428	0.428	0.432	0.428	0.424
	2nd		0.424	0.420	0.415	0.420	0.424
	3rd		0.428	0.420	0.407	0.407	0.420
	4th			0.428	0.398	0.398	0.407
	5th				0.390	0.394	0.403
	6th				0.390	0.390	0.398
	7th				0.390	0.386	0.394
	8th				0.390	0.386	0.390
	9th				0.398	0.386	0.390
	10th				0.407	0.386	0.390
	11th					0.386	0.390
	12th					0.386	0.390
	13th					0.386	0.390
	14th					0.386	
	15th					0.386	
Spacing Between Directors, λ		0.20	0.20	0.25	0.20	0.20	0.308
Gain, dBd		7.1	9.2	10.2	12.25	13.4	14.2
Reflector spaced 0.2 λ behind driven element.							

Up to this point, the structure of Yagi antennas with linear elements arranged in a single dimension, leading to linear polarization, is summarized. It is also possible to obtain a circularly polarized structure using a Yagi-Uda fashion. On the other hand, neither the historical article [52] nor the design procedure given in [53] (which cites [54]) provide a solution to obtain circular polarization with an antenna designed by the idea of Yagi-Uda. It is only explained in [51] and [55] that it is possible to design a circularly polarized array by a combination of horizontal and vertical Yagi antennas in a single supporting structure (boom), with a 90° phase shift between their feeds.

The details of the developed design including the feed structure to create circular polarization is explained in the following subsections.

3.2.2 Design Specifications

Design specifications are selected for an antenna that is suitable for a generic ground station setup operating in the VHF amateur radio band; for example, a setup to communicate with LEO satellites or a setup to establish an ARISS contact [56]. It is decided to design a Yagi antenna with circular polarization, unifying horizontal and vertical elements in a single boom with a phase difference of 90° between their feeds.

Although the required bandwidth for amateur radio operations around the center frequency is less than 20 kHz in the VHF amateur radio band, a simultaneous minimum bandwidth of 1 MHz for matching is specified as a requirement, to be in the safe side against detuning caused by wind, minor mechanical damages, etc., during operation. Center frequency tuning range is specified for a full coverage of the frequency band. Comparing 1.2 and 2.2 wavelength Yagi antennas in Table 3.1, it is seen that, with a cost of a unit wavelength increase in length, 2 dB additional gain can be obtained, which is considered as unworthy, considering that the extra length corresponds to approximately 2 m. It is decided to start the design with the provided 12.35 dBi (10.2 dBd) 6-element Yagi antenna, to limit the size at around 1.2 wavelength, due to mobility and compactness. With an added margin for the circular polarization arrangement and optimizations, the maximum length is specified as 3 m, while the gain value is specified as 11 dBi.

Specifications for the VHF antenna are given in Table 3.2.

Table 3.2: VHF directive antenna design specifications.

Specification	**Requirement**
Center Frequency Tuning Range	[144 146] MHz
S11 Bandwidth(< -10 dB)	> 1 MHz
Gain	> 11 dBi
Polarization	Circular
Maximum Length	3 m

3.2.3 Block Level System Design

Now, we present the block level system design to meet the requirements given in Table 3.2.

Circular polarization requirement can be met by using both vertical and horizontal elements together. The feeds of vertical and horizontal elements are supplied by dividing the transceiver signal path into two equal power components. It is important to insert a phase shift of 90° between vertical and horizontal elements for circular polarization. The required phase shift can be created by placing vertial and horizontal elements with a quarter-wavelength offset and feeding them by equi-phase sources, or placing elements without any offset and creating the required 90° phase offset in the feeds [51].

Using a single sense of polarization to communicate with moving platforms can cause losses in the link budget, because of the different responses of the atmosphere to different polarizations and/or changing orientations of platforms. To solve the issue, two separate antennas with different senses of polarizations can be used through separate transceive channels. Alternatively, a polarization switch that changes the sense of the polarization of a single antenna can be used in the design. To have all alternatives according to the preferences, a mechanical construction that makes it possible to insert a polarization switch without a modification on the aluminum structure is considered. This leads to a design in which vertical and horizontal elements are placed with ap-

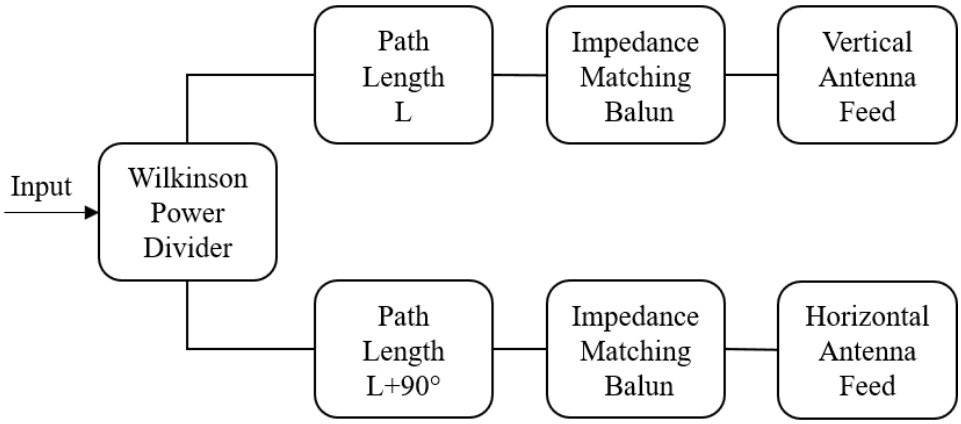

Figure 3.3: Circularly polarized Yagi antenna feed.

proximately no offset from each other. The required orthogonal phase shift to achieve circular polarization is planned to be inserted by using a quarter-wavelength longer coaxial line in one of the feed axes, in the first fabrication.

For a static sense of polarization, it is possible to use a quadrature hybrid, which may replace the power divider and phase shifter for a single structure. If there is a need for switchable polarization in a single antenna, a switched line delay line can be integrated into the system.

To facilitate fabrication, a linear half-wavelength dipole feed, which is a balanced structure, is considered as the most practical selection. It is known that the real part of the impedance of an infinitely thin half-wavelength dipole in free space is approximately $73\ \Omega$, while this value becomes lower when it is used in array structures. Also the finite radius of an antenna decreases its impedance [51]. The real and imaginary parts of the impedance should be calculated numerically by using a computational tool. After simulating the structure and calculating the port impedances, an impedance matching and balun circuit design is required to feed the antenna.

To summarize, the structure of the designed antenna can be investigated in three main parts: radiating structure, power divider, and impedance matching balun circuit. The block diagram of the design is given in Figure 3.3.

The radiating metal structure and the feed structure that consists of a power divider and matching balun circuits are explained in detail in the following subsections.

3.2.4 Design and Simulation of the Radiating Structure

Design of the radiating structure is started by the investigation of the available components in the market. For a low-cost fabrication, aluminum material is selected to be used in the fabrication of the antenna. The boom is selected as a hollow pipe with a square cross section, while the antenna elements are selected as rods with circular cross sections. The side length of the hollow pipe is 20 mm and the diameter of a rod is 8 mm. The boom and elements are physically connected via plastic clamps, which minimize mechanical efforts to fabricate the antenna.

The Yagi antenna is parametrically modeled in ANSYS Electronics Desktop (HFSS). For circular polarization, the model is duplicated with 90° rotation around the axis of the boom. The offset between the vertical and horizontal elements are taken as the minimum possible mechanical limit, which corresponds the width of the plastic clamps. The plastic clamps are modeled as boxes under the antenna elements, slightly different from the real case, to decrease the simulation time. The feeds are modeled by two separate lumped ports, with 90° phase shift between them. The simulation model can be seen in Figure 3.4.

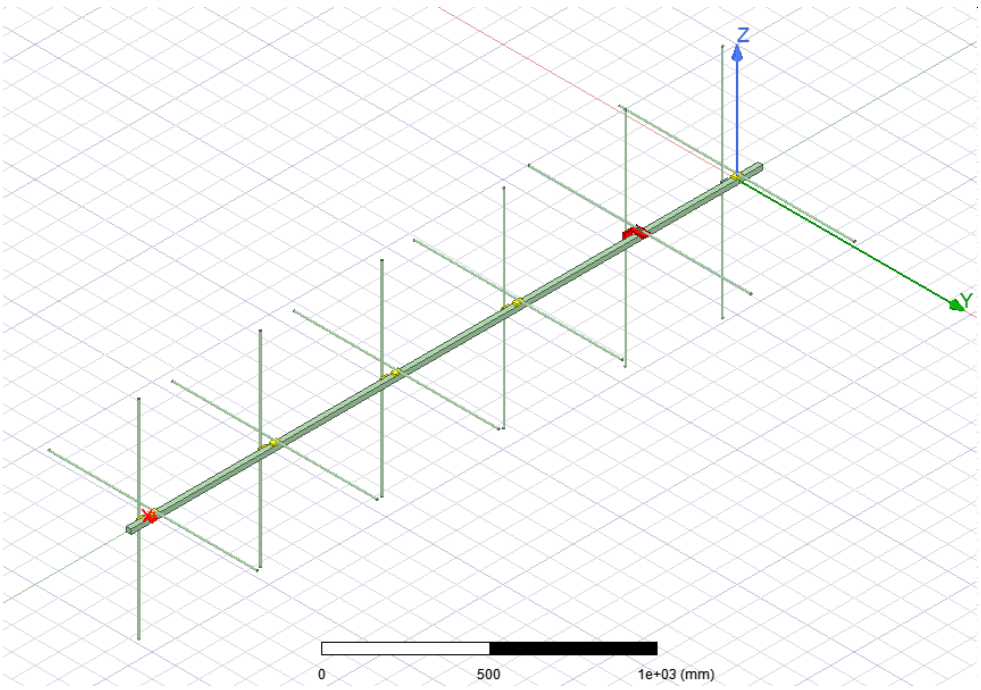

Figure 3.4: Circularly polarized Yagi antenna modeled in ANSYS HFSS.

Parameters are initialized in accordance with the empirical design guidelines given in [53] and [54]. The length parameters are defined in terms of the wavelength of the selected design frequency. The initial design frequency is taken as 145.5 MHz, to optimize the antenna for an ARISS contact, which occurs between 145 MHz and 146 MHz. The simulated gain plots at different frequencies can be seen in Figure 3.5. It is observed that the minimum back lobe and the maximum main lobe are observed in 148 MHz, which is slightly higher than the intended frequency, which is expected due to the need for compensation for the metallic boom.

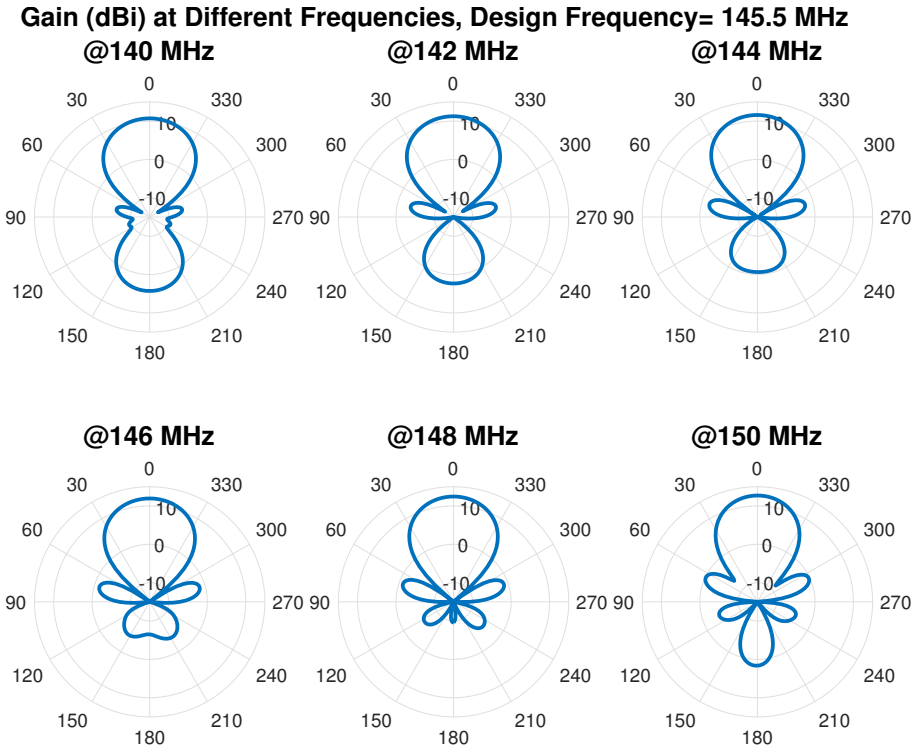

Figure 3.5: Gain of the initial design at different frequencies.

Gain pattern optimization of the structure is made by sweeping the variable of the design frequency. The patterns at 145.5 MHz by using different design frequencies are given in Figure 3.6. A sweeping step of 1.5 MHz is preferred, which is approximately 1% of the center frequency. The design frequency of 144 MHz is selected as optimum, because of the relatively low sidelobe and backlobe levels for this design.

Finer sweep for the design frequency is not preferred, considering possible fabrication tolerances. The length values of the directors and reflector with the design frequency of 144 MHz are further rounded for fabrication. A minimum sensitivity of

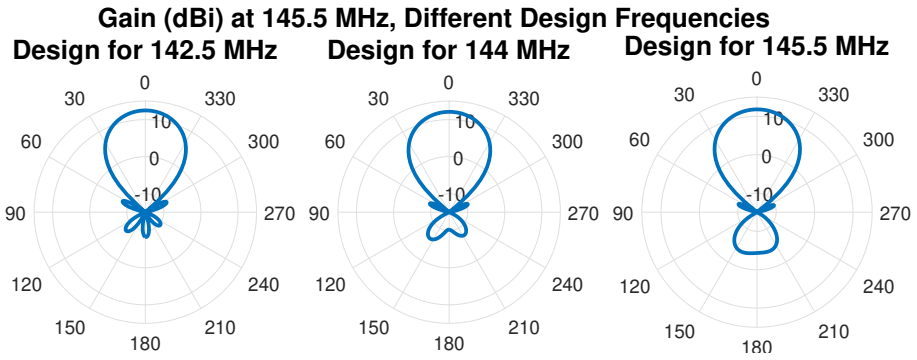

Figure 3.6: Gain at 145.5 MHz for different design frequencies.

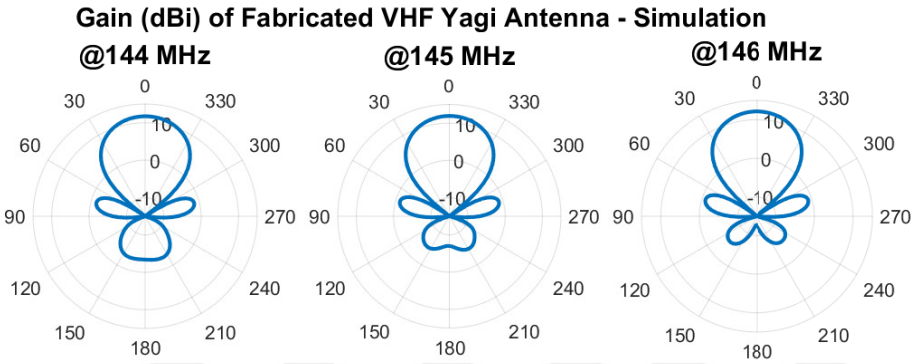

Figure 3.7: Gain simulation of the VHF Yagi prepared for fabrication.

5 mm is used for rounding. The gain patterns of the final structure at three different frequencies are given in Figure 3.7.

After the optimization of the gain pattern by sweeping the design frequency, the length of the feed elements is optimized for matching. This optimization has no visible effect on the radiation pattern, when the rest of the structure is not modified. As the expected port impedance is lower than 50 Ω, the port impedance in the simulation environment is changed. Specifically, 30 Ω impedance is selected for each port, as further explained in the next subsection. The return loss plots obtained with the feed length sweep are given in Figure 3.8. As can be seen from simulation results, it is advantegous to use telescopic feed elements to tune the antenna, when fabricated. Optimized sizes of the elements and spacing distances are given in Table 3.3.

As a final step in the HFSS simulation, models with a ground plane are prepared. The antenna is placed on an infinitely large ground plane with an angle of 45°. The

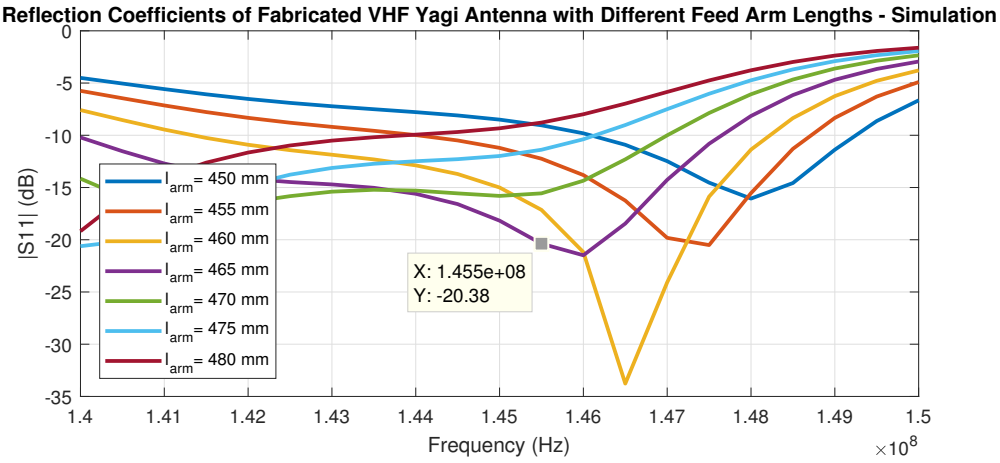

Figure 3.8: Simulated reflection coefficient curves for the VHF Yagi antenna prepared for fabrication with different feed arm lengths.

Table 3.3: Fabricated VHF Circularly Polarized Yagi antenna.

Fabricated Circularly Polarized Yagi Antenna for VHF Band		
Main Material		Aluminum
Clamp Material		Polypropylene (Insulating)
Boom Length, mm		2600
Rectangular Boom Side Length, mm		20
Antenna Element Diameter, mm		8
Offset Between Hor. and Ver. Elements, mm		40
Driven Element Arm Length, mm		465 (Telescopic tunable)
Driven Element Center Gap, mm		20
Length of Reflector, mm		1005
Length of Director, mm	1st	890
	2nd	875
	3rd	875
	4th	890
Spacing of Directors, mm		520
Spacing of Reflectors (Behind Feed), mm		415
Simulated Gain in Free Space @145.5 MHz, dBi		11.9

prepared model where the antenna is placed 1 m above the ground plane is shown in Figure 3.9, together with the corresponding gain simulation result. It is observed that, nulls are vanished, the reflection coefficient stays below -15 dB, and the maximum gain alteration is less than -1 dB at the boresight direction in the simulations where the VHF Yagi antenna is elevated 1 m and 2 m from ground. The antenna functionality is not changed in this scenarios. The optimization process conducted in this study seems to be sufficient to decide on the design parameters to be used in fabrication, when the integration platform is not known for sure.

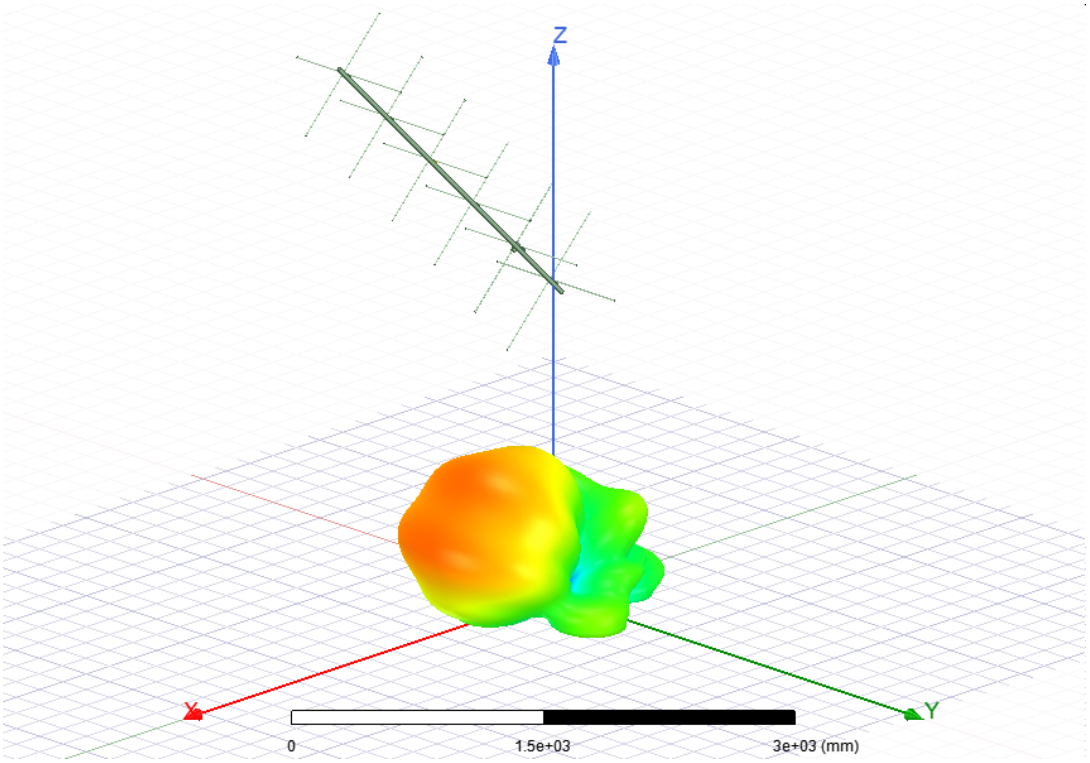

Figure 3.9: VHF Yagi simulation on top of the infinite ground plane.

3.2.5 Design and Simulation of the Feed Structure

The feed structure of the circularly polarized Yagi antenna consists of a power divider and an impedance matching balun together with interconnection cables, as shown in Figure 3.3. The well-known Wilkinson power divider [57] and a quarter-wave transformer [58] are prefered for their simple fabrications. The structure elements are simulated in NI AWR simulation environment. The separately simulated structures

are combined to obtain the system response at the end. To fabricate easily, it is aimed to use low-cost components, which are easily found in the market. To realize the design with minimum efforts, 75 Ω CATV coaxial cables are used as transmission lines.

Design details of both structures are included in the following subsections.

3.2.5.1 Impedance Matching Balun: Quarter-Wave Transformer with Ferrite Bead

Quarter-wave transformer operation can be understood easily, when the transmission line impedance equation is considered as

$$Z_{in} = Z_0 \frac{Z_L + jZ_0 \tan(\beta l)}{Z_0 + jZ_L \tan(\beta l)}, \tag{3.1}$$

where Z_{in} is the input impedance at the measurement point towards the load, Z_L is the load impedance, Z_0 is the characteristic impedance, $\beta = 2\pi/\lambda$ is the propagation constant, and l is the length of the transmission line between the load and measurement point. The situation is depicted in Figure 3.10.

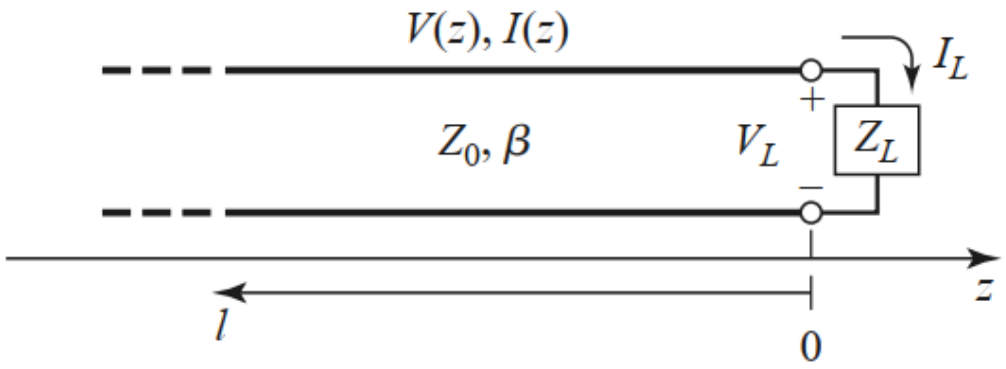

Figure 3.10: Transmission line terminated with a load [58].

The choice of length $l = \lambda/4$ has a special result that is very useful for matching loads to desired impedances. With such a selection of the length, the input impedance at the limit becomes

$$\lim_{l \to \frac{\lambda}{4}} Z_{in} = Z_0 \frac{Z_L + jZ_0 \tan(\frac{2\pi}{\lambda}\frac{\lambda}{4})}{Z_0 + jZ_L \tan(\frac{2\pi}{\lambda}\frac{\lambda}{4})} = Z_0 \frac{Z_L + jZ_0 \tan(\frac{\pi}{2})}{Z_0 + jZ_L \tan(\frac{\pi}{2})} = \frac{{Z_0}^2}{Z_L}. \tag{3.2}$$

Reorganizing Equation 3.2, the characteristic impedance of a quarter-wave transmission line that perfectly matches an input port with impedance Z_{in} to a termination with impedance Z_L can be found as

$$Z_0 = \sqrt{Z_{in} Z_L}. \tag{3.3}$$

Hence, to minimize the reflection coefficient between the load and port, one can use a transmission line of quarter wavelength (with a characteristic impedance of Z_0 calculated in Equation 3.3) between them. This matching structure is called as a quarter-wave transformer.

In this study, a quarter-wave transformer that matches $30\ \Omega$ load impedance to $50\ \Omega$ port impedance is considered to match the designed Yagi antenna to radio systems. By inserting the values into Equation 3.3, the required characteristic impedance for a quarter-wave transmission line is calculated as $Z_0 = \sqrt{50 \times 30} = 38.73\ \Omega$. By using a parallel connection of two $Z_0 = 75\ \Omega$ coaxial cables, it is possible to obtain a $Z_0 = 37.5\ \Omega$ transmission line, which is approximately equal to the required value.

A simulation model is prepared for the quarter-wave transformer to match $30\ \Omega$ to $50\ \Omega$, as seen in Figure 3.11. A differential impedance of $30\ \Omega$ (for antenna feed) is obtained by inserting two $15\ \Omega$ single-ended ports to the center-conductor and outer-conductor connections of the parallel coaxial transmission lines. It is desired to have a well-matched structure indicated by a low S11 value. The transfer ratios, i.e., S21 and S31, are expected to be equal to each other with a value of -3 dB, since there is no loss or amplitude unbalance modeled in the simulation environment, while they exist in coaxial transmission lines in real life. The transfer angles are expected to be 180° out of phase due to the complementary connections of the coaxial transmission lines, one port is connected to the inner conductors while the other is connected to outer conductors of the parallel connected cables. The simulation results, which comply with the theoretical expectations, are given in Figure 3.12. It is observed that the structure designed for the center frequency of 145.5 MHz shows similar performance in the UHF band, i.e., when the frequency is three times the frequency in the VHF band. The length of the transformer in the UHF band becomes three-quarter wavelength, which has a transfer characteristics like a quarter wavelength, since the difference is half wavelength.

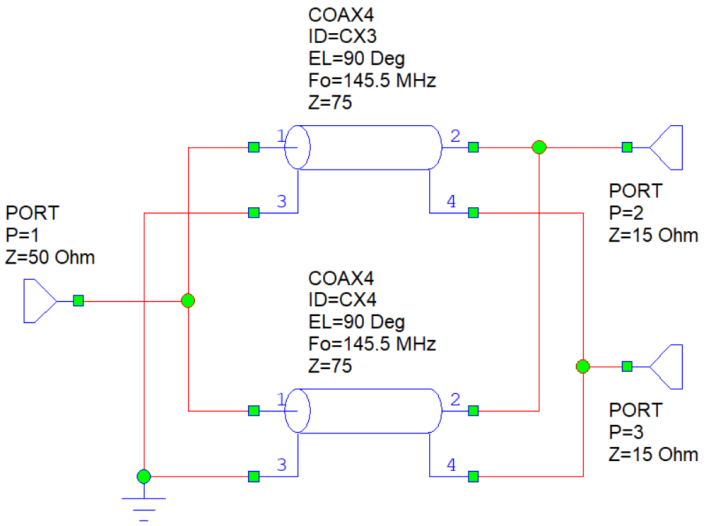

Figure 3.11: Quarter-wave transformer simulation model.

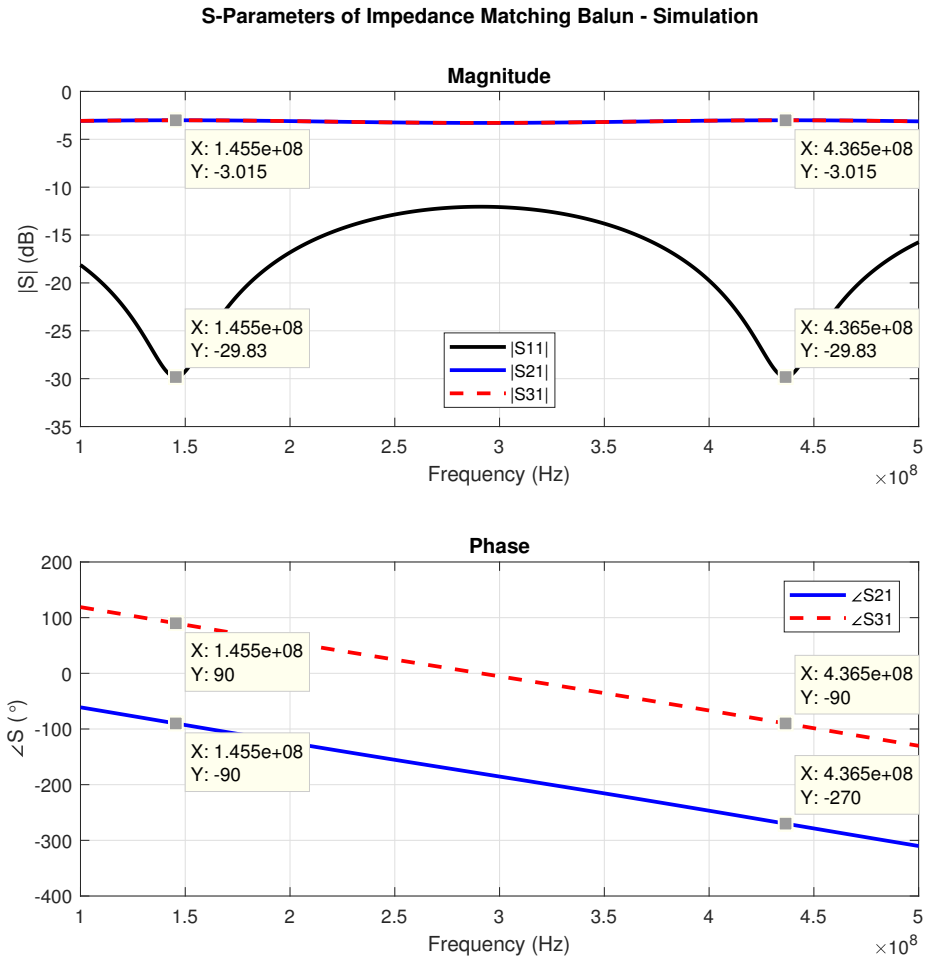

Figure 3.12: Quarter-wave transformer simulation results.

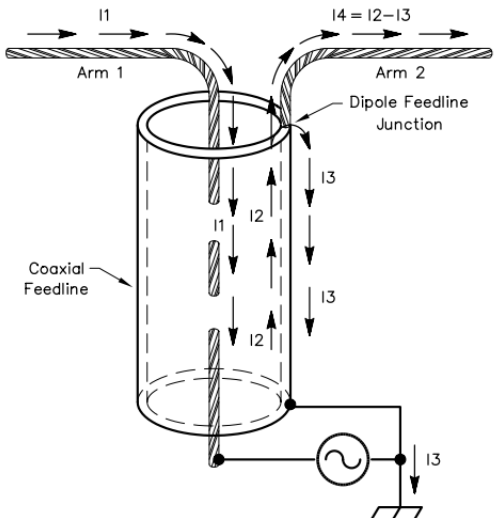

Figure 3.13: Currents on a coaxial fed dipole antenna [51].

Figure 3.14: Snap-on ferrite beads [60].

The simulation results for the designed quarter-wave transformer demonsrate a succesful match between the antenna and feed. In addition to the matching, however, balun operation is needed at the antenna feed point. Due to the finite value of the skin depth, unwanted currents flow on the outer side of the outer conductor of the coaxial line. Because of this, the arms of the feed element become unbalanced. The situation is depicted in Figure 3.13, where $I1$ and $I2$ represent the desired equal-magnitude and opposite-phase currents, while $I3$ is the unwanted common mode leakage current.

To solve the issue, snap-on ferrite beads, structures that prevent current flow at the outer side of the coaxial cable, can be used [59]. This way, the arms of the feed are fed by equal amounts of currents. This is the easiest solution to cancel the unwanted current I3 in Figure 3.13 to make the magnitudes of $I1$ and $I2$ equal. Examples of snap-on ferrite beads are shown in Figure 3.14 [60]. A suitable product that works well in the desired operation frequency and that mechanically fits to the fabricated quarter-wave transformer is selected and employed.

3.2.5.2 Wilkinson Power Divider

Two-way Wilkinson power divider (Figure 3.15), a structure that divides the input signal into two equal-magnitude and equal-phase signals or combines two equal-magnitude and equal-phase signals without any loss or reflection, is analysed by using even-odd analysis technique, as explained in [58]. To conduct the analysis with ease, an equivalent symmetrical circuit is drawn, then a symmetry line is used to obtain even and odd excited equivalent half-circuits. Normalized half-circuits for the even and odd excitations are given in Figure 3.16.

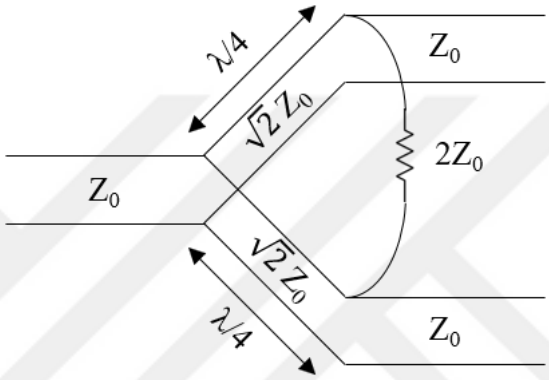

Figure 3.15: Two-way Wilkinson power divider.

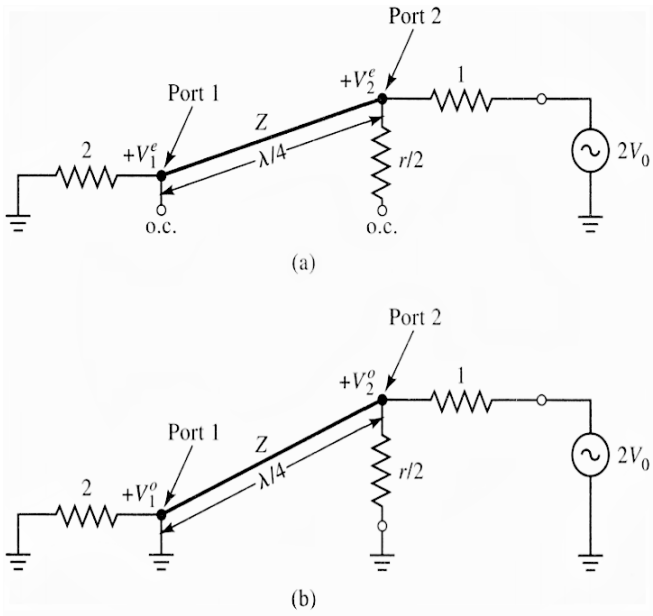

Figure 3.16: Half-circuits for (a) even excitation, (b) odd excitation [58].

The analysis steps include quarter-wave transformers, as formulated in Equation 3.3. Also, the equation for the voltage on the transmission line with changing measurement position, i.e.,

$$V(x) = V^+(x) + V^-(x) = |V^+(x)|(e^{-j\beta x} + \Gamma e^{j\beta x}), \tag{3.4}$$

is used in the analysis. In Equation 3.4, V^+ is the voltage of the forward propagating wave, V^- is the voltage of the backward propagating wave, Γ is the reflection coefficient, β is the propagation constant, and x is the position. With the analysis of the even mode, we obtain $V_2^e = V_0$ and $V_1^e = -jV_0\sqrt{2}$, while the analysis of the odd mode leads to $V_2^o = V_0$ and $V_1^o = 0$.

As the following step, the input impedance is found easily without conducting the even-odd analysis. When the output ports of the Wilkinson power divider in Figure 3.15 is terminated with Z_0 loads, there is no current flow through the isolation resistor, and it can be replaced with an open circuit. Then, the input impedance, which is the parallel combination of two output ports with quarter-wave transformers, is calculated by using Equation 3.1 as

$$\lim_{l \to \frac{\lambda}{4}} Z_{in} = \frac{1}{2}\sqrt{2}Z_0 \frac{Z_0 + j\sqrt{2}Z_0 \tan(\frac{2\pi}{\lambda}\frac{\lambda}{4})}{\sqrt{2}Z_0 + jZ_0 \tan(\frac{2\pi}{\lambda}\frac{\lambda}{4})} = Z_0, \tag{3.5}$$

leading to

$$\Gamma_{in} = \frac{Z_{in} - Z_0}{Z_{in} + Z_0} = 0 \tag{3.6}$$

for the input reflection coefficient. By the even-odd and input impedance analyses, it is seen that all ports of the Wilkinson power divider are matched, resulting in zero reflection coefficient in the design frequency. Also, the transfer coefficient between Port 1 and Port (i.e., S21) is calculated as

$$\text{S21} = \frac{V_1^e + V_1^o}{V_2^e + V_2^o} = -j\sqrt{2}, \tag{3.7}$$

which is equal to S12 due to reciprocity and equal to S31 and S13 due to symmetry, implying a -3 dB ratio and 90° phase shift.

A simulation model in NI AWR environment is prepared (Figure 3.17), by using the coaxial transmission lines of impedance $75\ \Omega$ in the design, which have slightly larger impedance than the optimum selection of $70.7\ \Omega$.

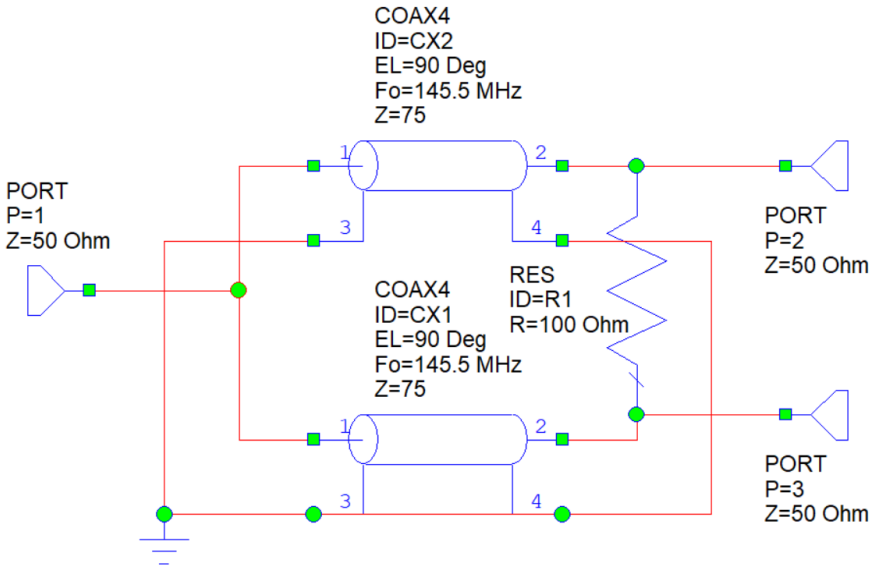

Figure 3.17: Wilkinson power divider simulation model.

Simulation results of the Wilkinson power divider are given in Figure 3.18. It is seen that the input and output reflection coefficients, as well as the isolation between the output ports are better than -20 dB (at the desired frequencies), while the transfer magnitude is at around -3 dB, as expected. The advantage of using this structure is having a power divider that works in both VHF and UHF bands; this is an issue in quarter-wave transformer explained in the previous subtitle.

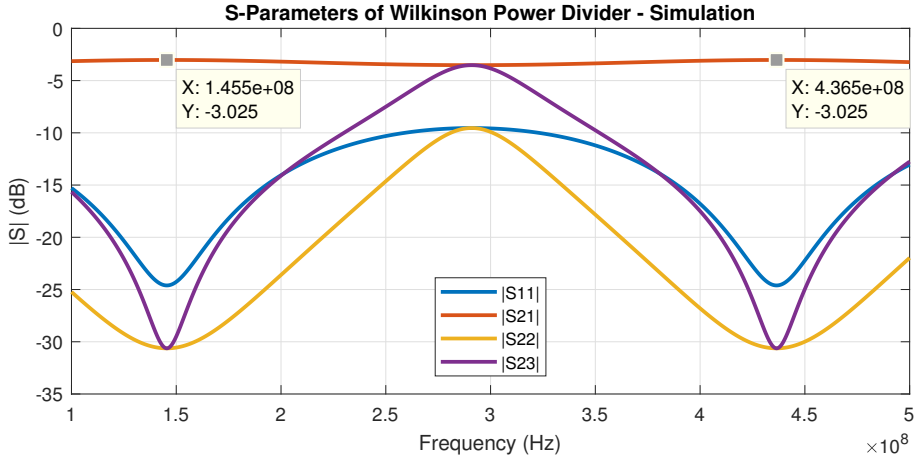

Figure 3.18: Wilkinson power divider simulation results.

3.2.5.3 Combined Feed Structure: Power Divider and Impedance Matching Balun

An overall simulation model, which represents the design in Figure 3.3, is prepared as shown in Figure 3.19. The simulation models in the previous two subsections are combined to obtain the overall system model, while $50\ \Omega$ transmission lines are placed between them, one of which is 90° longer than the other to obtain circular polarization.

The simulation results are given in Figure 3.20. Results show that the input reflection coefficient is low, the transfer magnitude to each antenna arm is equal to -6 dB, isolation between the arms of the different antennas are high, and the transfer phase values are appropriate to feed the circularly polarized dipole pair at the desired center frequency.

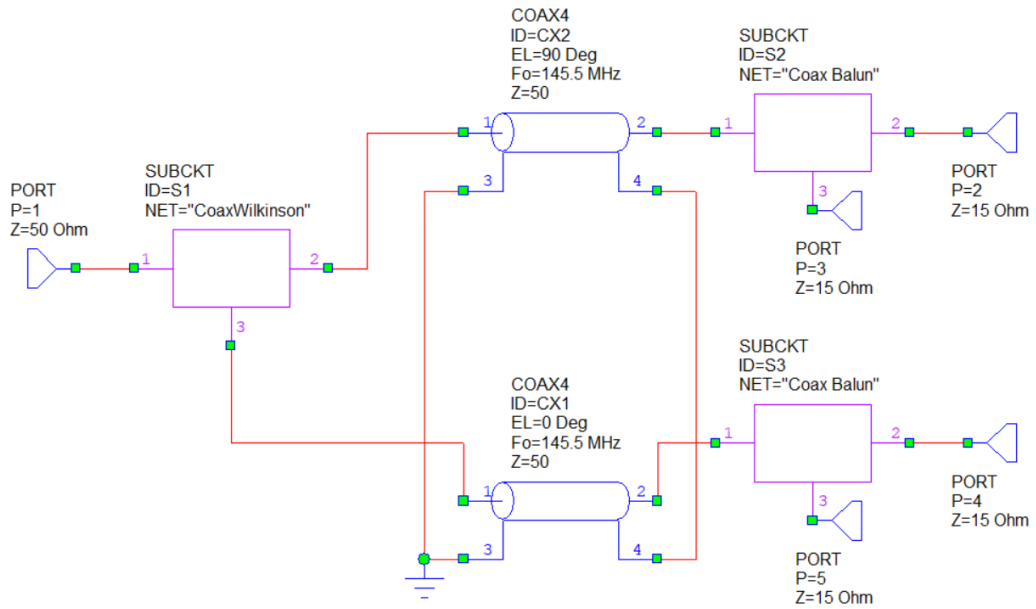

Figure 3.19: Overall system simulation model.

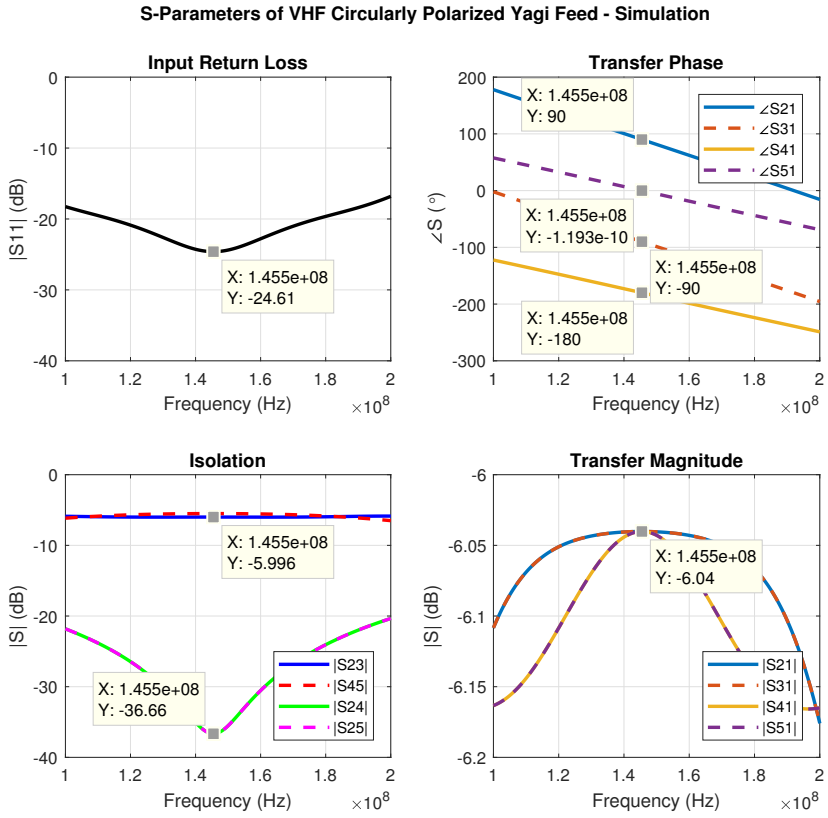

Figure 3.20: Overall system simulation results.

3.2.6 Fabrication and Measurement

Fabrication of the antenna is performed by a team of amateur radio enthusiasts, using aluminum rods and home-brew PCB fabrication techniques. BNC-type connectors are used in this first prototype. PCB fabrication required for the Wilkinson power divider is completed by thermal mask transfer and chemical etching. The prepared mask for the Wilkinson power divider PCB is shown in Figure 3.21. The fabricated power divider and its S-parameter measurement results are given in Figure 3.22 and Figure 3.23, respectively.

The impedance matching balun is fabricated by $75\ \Omega$ CATV cables, snap-on ferrite beads, and BNC type coaxial connectors, as shown in Figure 3.24. The connections between the impedance matching balun and antenna feeds are maintained by crimped electrical terminals. Radiating parts of the antenna are fabricated by aluminum rods, while hydraulic pipe clamps are preferred as insulating connection pieces to attach radiating elements to the antenna boom. The fabricated antenna on a tripod is shown in Figure 3.25. S-parameter measurement of the antenna with impedance matching balun is given in Figure 3.26.

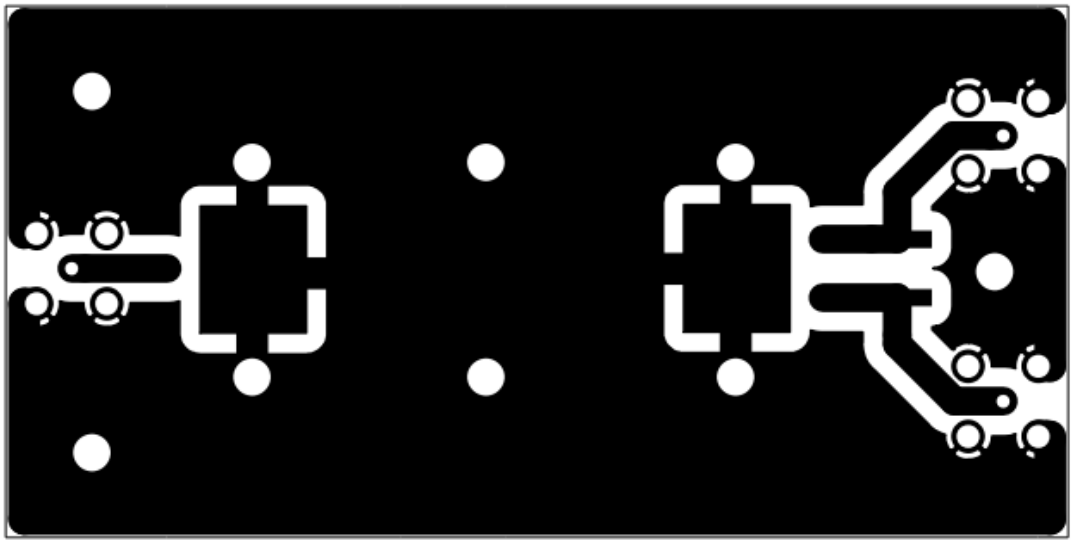

Figure 3.21: Prepared mask for the Wilkinson power divider PCB.

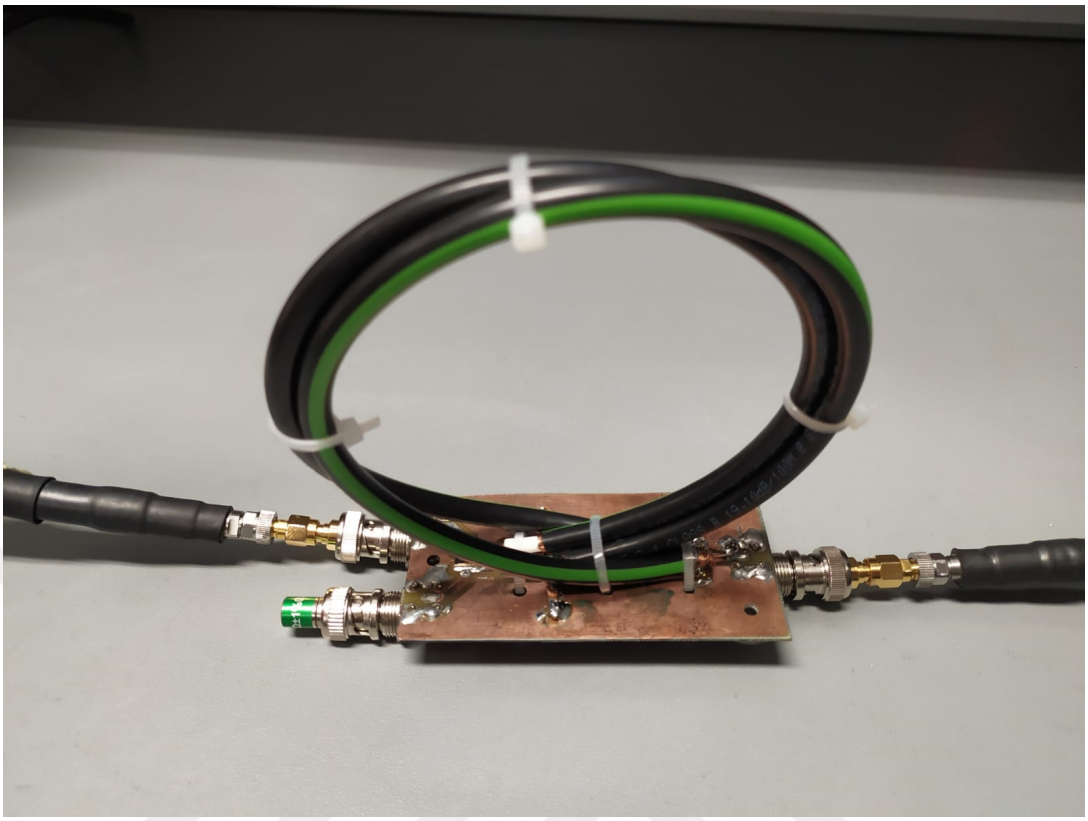

Figure 3.22: Fabricated Wilkinson power divider.

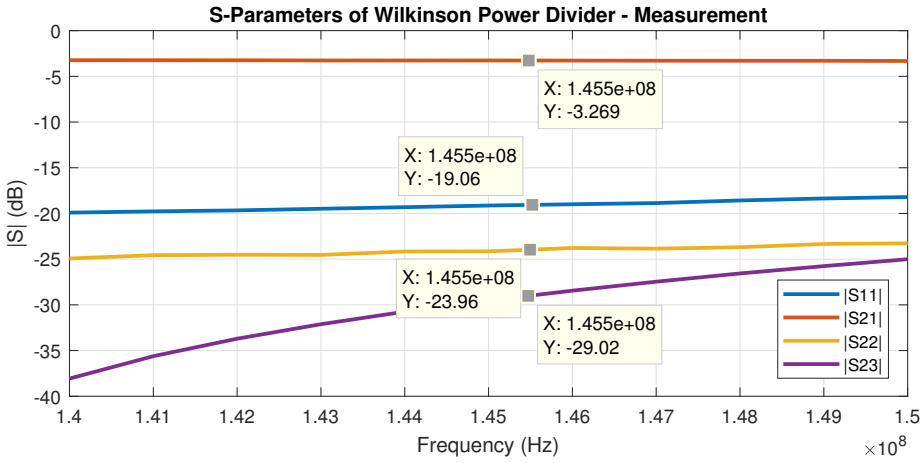

Figure 3.23: Wilkinson power divider measurement results.

Figure 3.24: Fabricated impedance matching balun.

Figure 3.25: Fabricated Yagi antenna on a tripod.

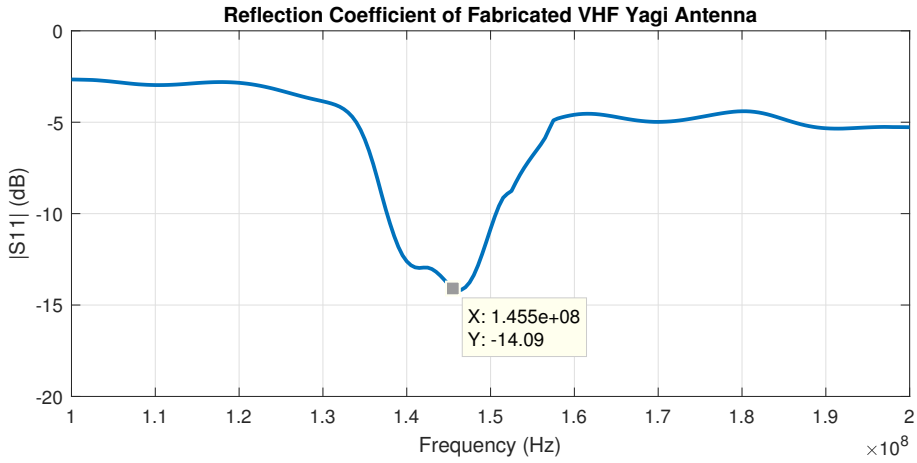

Figure 3.26: Measurement results for the fabricated Yagi antenna.

3.2.7 Field Test

The fabricated antenna is used to receive a Slow-Scan TV (SSTV) image from International Space Station, on 05.08.2020, 19:55 to 19:57 in OSTİM, Ankara, at 145.800 MHz. The antenna is placed on the top of a tripod and rotated manually to follow ISS passing above, as shown in Figure 3.27 [61]. An Icom 910H radio (sensitivity of -121 dBm), together with 3 m long RG58 coaxial cable (with 1 dB insertion loss) are used to receive signals from ISS, without an additional LNA. A successfully received SSTV image is given in Figure 3.28. The image does not include any dead regions, which are typically observed in previous SSTV experiments with mobile whip antennas.

3.3 Design of a Circularly Polarized UHF Yagi Antenna

A circularly polarized, high-gain UHF Yagi antenna is designed, for the completeness of this study. The same design steps as in the VHF case are followed to obtain an antenna that operates in the UHF band. The resulting design has 2×17 elements, has 15.7 dBi gain, and is 2.5 m long, i.e., it is not larger than the designed VHF antenna. Gain and reflection coefficient simulation results are given in Figure 3.29 and Figure 3.30, respectively. Optimized sizes of the elements and spacing distances are further listed in Table 3.4.

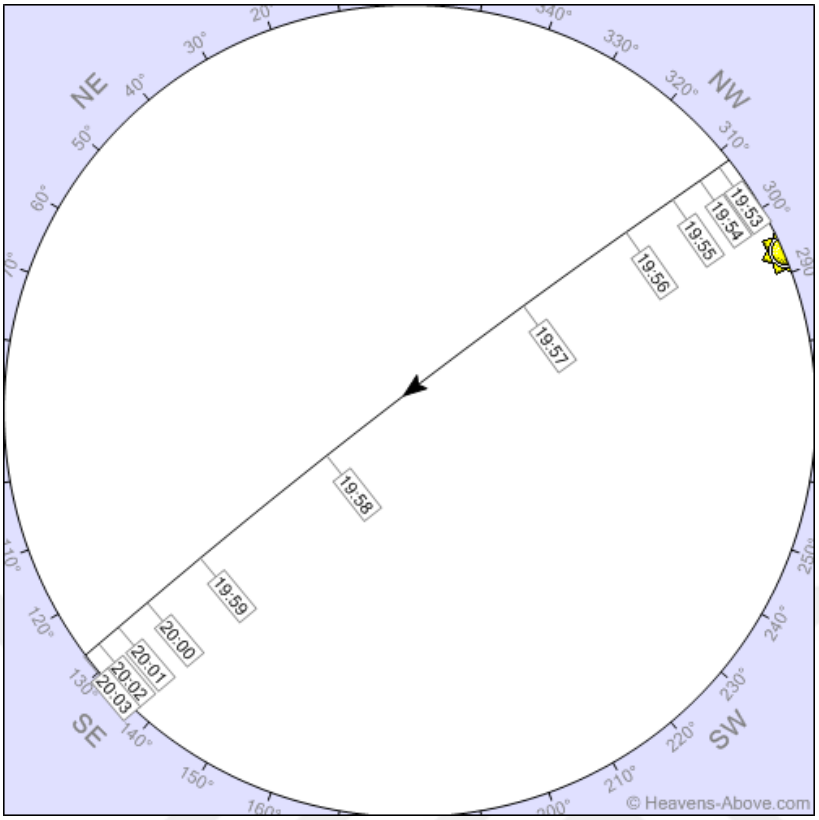

Figure 3.27: ISS pass details for OSTİM, Ankara on 05.08.2020 [61].

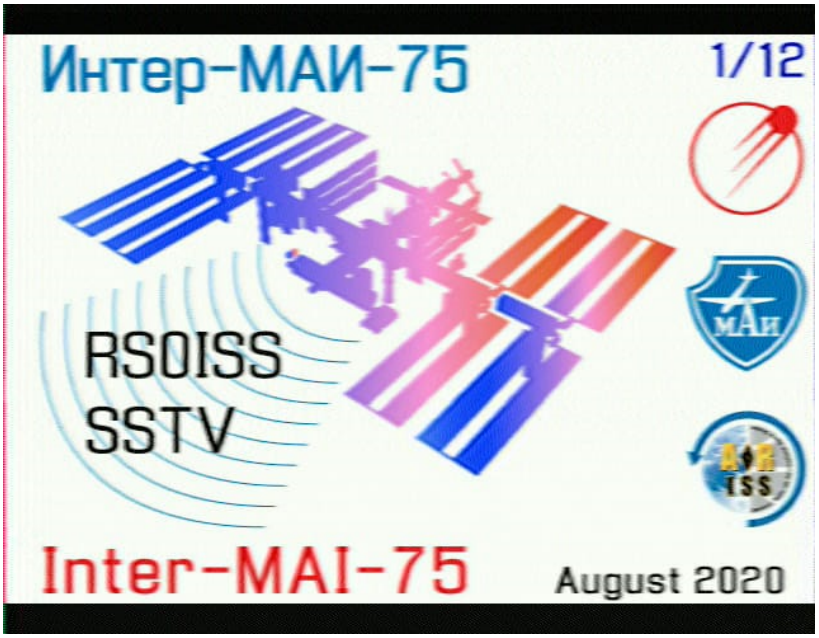

Figure 3.28: Received SSTV image.

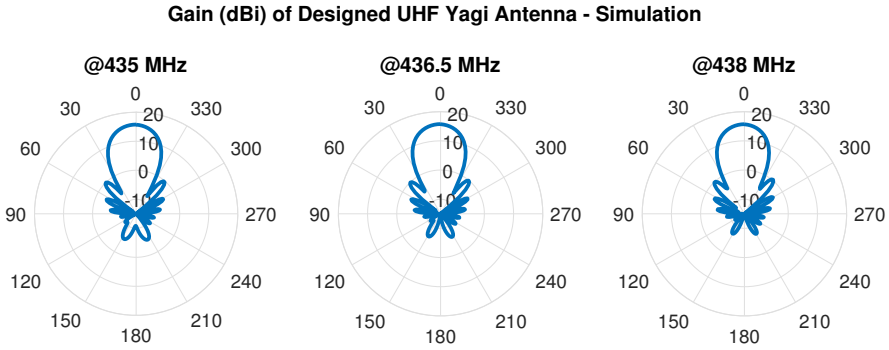

Figure 3.29: Gain simulation of the designed UHF Yagi antenna.

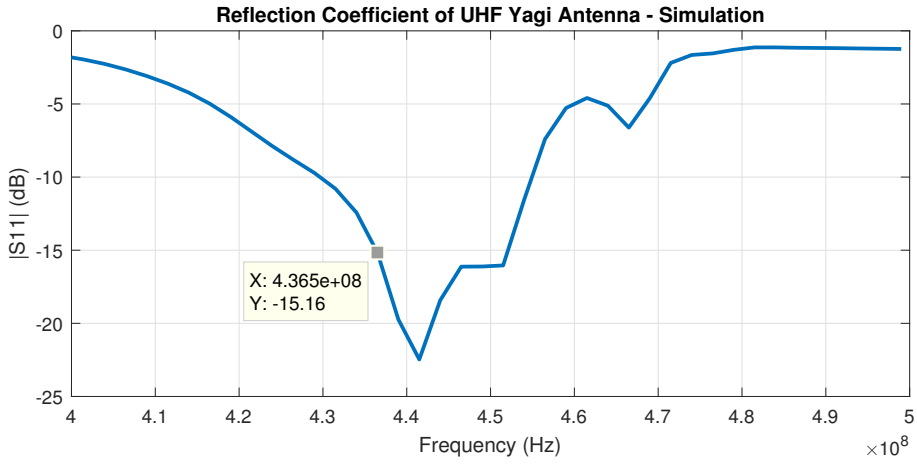

Figure 3.30: Reflection coefficient simulation results for the designed UHF Yagi antenna.

Table 3.4: Designed UHF Circularly Polarized Yagi antenna.

Designed Circularly Polarized Yagi Antenna for UHF Band		
Main Material		Aluminum
Clamp Material		Insulating Plastic
Boom Length, mm		2500
Rectangular Boom Side Length, mm		20
Antenna Element Diameter, mm		8
Offset Between Hor. and Ver. Elements, mm		40
Driven Element Arm Length, mm		140
Driven Element Center Gap, mm		20
Length of Reflector, mm		330
Length of Director, mm	1st	290
	2nd	285
	3rd	280
	4th	270
	5th	270
	6...15th	265
Spacing of Directors, mm		135
Spacing of Reflectors (Behind Feed), mm		135
Simulated Gain in Free Space @436.5 MHz, dBi		15.7

CHAPTER 4

CONCLUSIONS AND FURTHER WORKS

CubeSat ground station and on-board antenna systems are designed, simulated, and fabricated in this study. The measurement results are obtained and used to support the simulation results.

A circularly polarized UHF turnstile antenna is fabricated, to be used on a CubeSat platform after the realization of a mechanical deployment structure and performing environmental tests. Pattern optimization is conducted by changing the orientations of the antenna arms to meet the requirements of different scenarios. V/UHF dual-band turnstile antenna is designed by inserting LC-traps onto the antenna arms. An optimization similar to the single-band antenna module will be conducted as a further study. According to our plans, the feed circuit of the dual-band turnstile antenna will be fabricated by replacing the hybrid coupler in the single-band circuit with Innovative Power Products' IPP-7057, which operates in the frequency range of 100-520 MHz. The antenna arms will be fabricated from conducting strips, and small PCBs including the components of the traps will be inserted at the desired positions, by using the simulation results and fine tuning in the laboratory. The hybrid coupler and balun components used in the PCB can further be replaced by printed structures, which will be a further improvement.

A circularly polarized VHF Yagi ground station antenna is fabricated to meet the requirements of general purpose CubeSat ground stations and ARISS contacts. Low-cost home-brew prototyping techniques are succesfully used for the realization of the designed structure in the simulation environment. For high power handling and higher environmental durability, the Wilkinson power divider and impedance matching balun of the ground station antenna will further be fabricated by using Type-N connectors,

while the connections between them will be maintained by LMR400-type cables. The circuits will be covered by a metallic box, which will be mounted onto the boom of the antenna. Tests with high levels of transmit power are required to prove the power handling capacity of the system. It is planned to fabricate the designed UHF antenna together with high power handling VHF antenna, and place both antennas together in a generic ground station setup, which will be used by TAMSAT members.

The practical experience gained during this study is valuable as a scientific approach to amateur radio antenna systems. It is observed that simple techniques used by amateur radio enthusiasts are beneficial if they are applied correctly. It is observed that the information presented by the well-known people in the amateur society, such as W4RNL, includes theoretical background and simulation results, showing the importance of theoretical design and simulations before any fabrication steps. The books published by accredited organizations, such as [51], are very important by explicitly providing reliable information to the enthusiasts.

Lessons learned from this study are important particularly for the people, who will try to design and fabricate similar systems, to identify the widely used false facts. For example, it is not possible to decrease the reflection coefficient of the telescopic antenna used in the first measurement session of the UHF turnstile system even though the length of the antenna is telescopically adjusted, due to the hinge placed near the antenna port. When measured by a multimeter's buzzer test function, continuity is observed. It is assumed for the hinge to maintain the electrical connection between the bottom and the tip of the telescopic antenna; however, the uncertain finite impedance at the connection position at the operation frequency can strongly deteriorate the antenna operation.. The best reflection coefficient result is obtained as -3 dB by tuning the length, which is a value not enough for a structure to be an antenna. Other than incorrectly designed components like the telescopic antenna, it is also important to verify the COTS component datasheets by measurements, in the case of a discrepancy, as observed in the plastic-case UHF antenna that required a tuning process. Another lesson learned from the fabrication of the on-board antenna is the importance of the thermal reliefs. Due to the lack of the thermal reliefs in the PCB, the soldering process of the pads that are connected to ground takes a long time, which harmed the components in the first fabrication process. To solve the issue, a soldering pro-

cess is performed in a DIY reflow oven which heats the whole circuit simultaneously, without melting the components thanks to the reduced process time.

It is advised that during the design of a ground station antenna system, the bottleneck should always be considered as the mechanical constraints. It is observed that the mechanical durability of the boom and the rod carrying the antenna is very important to continue operation during windy weather conditions. The antenna designer should always be aware of the mechanical limitations, ideally take support from mechanical designers. The transportation should also be considered, by dividing the long parts to several pieces, as in the case of a boom.

It is observed that the measurement devices designed for the use of amateur radio operators, such as analog SWR meters and analog power meters, provide accurate results when compared to costly professional measurement devices. The advantage of the professional devices appears when one tries to obtain numerically detailed measurement results in a wide frequency band.

Amateur radio setups might contain pieces with overperformance, such as giant antennas with high gain or amplifiers with output power in the order of kWs, although the link analysis results do not require. This issue is an advantage for receiver systems to obtain clear communications, whereas it is problematic for other transmitter systems trying to reach to the same receiver. The delivered signal from a transmitter to a receiver needs to be stronger than the other signals in the receiver environment (interference) for proper communications. Even though there are limitations on EIRP (effective isotropic radiated power) level of amateur stations, there are misuses. Designers should be aware of other transmitters and try to push the limits, while avoiding legal violations.

REFERENCES

[1] K. Lant, "Elon Musk: Launching a Satellite with SpaceX is $300 Million Cheaper," 2017. https://futurism.com/, accessed 2019-07-20.

[2] Spaceflight, "Schedule and Pricing," 2019. http://spaceflight.com/, accessed 2020-05-15.

[3] J. Fishman, "NASA Small Satellites to Demonstrate Swarm Communications and Autonomy," 2015. https://www.nasa.gov/, accessed 2020-03-10.

[4] E. Kulu, "Nanosats Database," 2019. https://www.nanosats.eu/, accessed 2019-10-06.

[5] E. Mabrouk, "What are SmallSats and CubeSats?," 2015. https://www.nasa.gov/, accessed 2020-03-10.

[6] CubeSat Standard, "CubeSat Developer Resources," 2019. http://www.cubesat.org/, accessed 2020-05-01.

[7] NASA CubeSat Launch Initiative, "CubeSat 101: Basic Concepts and Processes for First-Time CubeSat Developers," October 2017.

[8] A. Chin, R. Coelho, R. Nugent, R. Munakata, and J. Puig-Suari, "CubeSat: the pico-satellite standard for research and education," in *AIAA Space 2008 Conference & Exposition*, p. 7734, 2008.

[9] National University of Singapore Satellite Technology and Research Centre, "Galassia-2: A Student Developed CubeSat for Remote Sensing," 2020. https://online.ece.nus.edu.sg/star/, accessed 2020-07-15.

[10] K. Lemmer, "Propulsion for CubeSats," *Acta Astronautica*, vol. 134, pp. 231–243, 2017.

[11] J. Arlas and S. Spangelo, "GPS results for the Radio Aurora eXplorer II CubeSat

mission," in *51st AIAA Aerospace Sciences Meeting including the New Horizons Forum and Aerospace Exposition 2013*, pp. 1–8, 2013.

[12] ISIS Space, "VHF Uplink/UHF Downlink Full Duplex Transceiver," 2019. https://www.isispace.nl/product/isis-uhf-downlink-vhf-uplink-full-duplex-transceiver/, accessed 2020-03-10.

[13] B. Dinç, "TAMSAT CubeSat VHF/UHF Transponder V1.0," 2018. http://www.tamsat.org.tr/tr/tamsat-cubesat-vhf-uhf-transponder-v1-0/, accessed 2020-02-01.

[14] Clyde Space, "CPUT VUTRX Transceiver," 2019. https://www.clyde.space/products/14-cput-vutrx/, accessed 2020-03-10.

[15] D. Barbarić, J. Vuković, and D. Babic, "Link budget analysis for a proposed CubeSat Earth observation mission," in *2018 41st International Convention on Information and Communication Technology, Electronics and Microelectronics (MIPRO)*, pp. 0133–0138, 2018.

[16] B. Klofas and K. Leveque, "The future of CubeSat communications: transitioning away from amateur radio frequencies for high-speed downlinks," in *Proceedings of AMSAT Space Symposium*, 2012.

[17] S. K. Podilchak, D. Comite, B. K. Montgomery, Y. Li, V. Gómez-Guillamón Buendía, and Y. M. M. Antar, "Solar-panel integrated circularly polarized meshed patch for CubeSats and other small satellites," *IEEE Access*, vol. 7, pp. 96560–96566, 2019.

[18] E. Peral, E. Im, L. Wye, S. Lee, S. Tanelli, Y. Rahmat-Samii, S. Horst, J. Hoffman, S. H. Yun, T. Imken, and D. Hawkins, "Radar technologies for Earth remote sensing from CubeSat platforms," *Proceedings of the IEEE*, vol. 106, pp. 404–418, Mar. 2018.

[19] B. Carlsen, "Cornell University CubeSat for WSJ," 2017. https://www.brettcarlsen.com/blog/2017/10/3/cornell-university-cubesat-for-wsj/, accessed 2020-02-01.

[20] ISIS Space, "CubeSat Antenna System for 1U/3U," 2018. https://www.isispace.nl/product/cubesat-antenna-system-1u-3u/, accessed 2020-07-10.

[21] GOMSpace, "NanoCom ANT430," 2020. https://gomspace.com/shop/subsystems/communication-systems/nanocom-ant430.aspx/, accessed 2020-07-10.

[22] S. Gao, K. Clark, M. Unwin, J. Zackrisson, W. A. Shiroma, J. M. Akagi, K. Maynard, P. Garner, L. Boccia, G. Amendola, G. Massa, C. Underwood, M. Brenchley, M. Pointer, and M. N. Sweeting, "Antennas for modern small satellites," *IEEE Antennas and Propagation Magazine*, vol. 51, no. 4, pp. 40–56, 2009.

[23] J. Costantine, Y. Tawk, I. Maqueda, M. Sakovsky, G. Olson, S. Pellegrino, and C. G. Christodoulou, "UHF deployable helical antennas for CubeSats," *IEEE Transactions on Antennas and Propagation*, vol. 64, no. 9, pp. 3752–3759, 2016.

[24] Y. Rahmat-Samii, V. Manohar, and J. M. Kovitz, "For satellites, think small, dream big: a review of recent antenna developments for CubeSats," *IEEE Antennas and Propagation Magazine*, vol. 59, no. 2, pp. 22–30, 2017.

[25] J. Costantine, Y. Tawk, C. G. Christodoulou, J. Banik, and S. Lane, "CubeSat deployable antenna using bistable composite tape-springs," *IEEE Antennas and Wireless Propagation Letters*, vol. 11, pp. 285–288, 2012.

[26] M. Samsuzzaman, M. T. Islam, S. Kibria, and M. Cho, "BIRDS-1 CubeSat constellation using compact UHF patch antenna," *IEEE Access*, vol. 6, pp. 54282–54294, 2018.

[27] S. Marholm, "Antenna Systems for NUTS," Master's thesis, Norwegian University of Science and Technology, 2012.

[28] F. J. Severson, "An Overview of the Petite Amateur Navy Satellite (PANSAT) Project," Master's thesis, Naval Postgraduate School, Monterey, California, 1995.

[29] D. A. Ellrick, “An Antenna Design for PANSAT Using NEC,” Master’s thesis, Naval Postgraduate School, Monterey, California, 1991.

[30] E. Karapinar, “Modification and Verification of an Antenna Design for Petite Amateur Navy Satellite (PANSAT) Using NEC,” Master’s thesis, Naval Postgraduate School, Monterey, California, 1995.

[31] G. J. Smilowitz, “Final Design, Integration and Validation of the PANSAT Antenna System,” Master’s thesis, Naval Postgraduate School, Monterey, California, 1997.

[32] E. S. Moghaddam and S. Amiri, “Development of separated turnstile antenna for space applications,” *IEEE Antennas and Propagation Magazine*, vol. 50, pp. 84–93, Aug. 2008.

[33] S. X. Ta, I. Park, and R. W. Ziolkowski, “Crossed dipole antennas: a review,” *IEEE Antennas and Propagation Magazine*, vol. 57, no. 5, pp. 107–122, 2015.

[34] S. D. Kulkarni and S. N. Makarov, “A circularly polarized UHF antenna at 550-700 MHz,” in *2007 IEEE Antennas and Propagation Society International Symposium*, pp. 2981–2984, 2007.

[35] I. Radnović, A. Nešić, and B. Milovanović, “A new type of turnstile antenna,” *IEEE Antennas and Propagation Magazine*, vol. 52, no. 5, pp. 168–171, 2010.

[36] K. Keyghobad, J. M. Baabuei, and T. Heydari, “Design & fabrication of turnstile antenna with feed network optimization for LEO satellites,” in *2007 6th International Conference on Antenna Theory and Techniques*, pp. 286–288, 2007.

[37] D. D. Reuster and K. J. Cybert, “A high-efficiency broadband HF wire-antenna system,” *IEEE Antennas and Propagation Magazine*, vol. 42, no. 4, pp. 53–69, 2000.

[38] W. Edson, “Broadband trapped multiple-wire antennas,” in *1981 Antennas and Propagation Society International Symposium*, vol. 19, pp. 586–589, 1981.

[39] Texas Instruments, “CC2592 - 2.4 GHz Range Extender Datasheet,” 2014. `https://ti.com/`, accessed 2020-04-15.

[40] D. R. Glover, "Satellite radio communications fundamentals and link budgets," in *Handbook of Satellite Applications* (S. Pelton Joseph N. and Madry and C.-L. Sergio, eds.), pp. 431–462, New York, NY: Springer International Publishing, 2017.

[41] P. Poshala, "Signal Chain Noise Figure Analysis," tech. rep., Texas Instruments, 2014.

[42] US4ICI, "Sequencer PCB for LNA, PA, RF-Relays, Transceiver," 2016. `https://vhfdesign.com/other/sequencer-pcb.html/`, accessed 2020-04-10.

[43] Graw Radiosondes, "Ground Station Equipment." `https://www.graw.de/products/groundstation-equipment/`, accessed 2020-04-15.

[44] H. Heidt, J. Puig-Suari, A. S. Moore, S. Nakasuka, and R. J. Twiggs, "CubeSat: a new generation of picosatellite for education and industry low-cost space experimentation," in *AIAA/USU Small Satellite Conference Proceedings V-5*, 2000.

[45] SatNOGS Network. `https://network.satnogs.org/`, accessed 2020-04-15.

[46] International Telecommunication Union Radiocommunication Bureau, *Handbook on Amateur and Amateur-Satellite Services*. International Telecommunication Union, 2014.

[47] W. F. Dabberdt and H. Turtiainen, "Observations platforms, radiosondes," in *Encyclopedia of Atmospheric Sciences (Second Edition)* (G. R. North, J. Pyle, and F. Zhang, eds.), pp. 273–284, Oxford: Academic Press, 2nd ed., 2015.

[48] J. E. Allnutt, "Satellite Earth station antenna systems and system design," in *Handbook of Satellite Applications*, pp. 567–601, Springer International Publishing, 2017.

[49] J. Laheurte, *Compact Antennas for Wireless Communications and Terminals: Theory and Design*. John Wiley & Sons, 2012.

[50] H. T. Friis, “A note on a simple transmission formula,” *Proceedings of the IRE*, vol. 34, no. 5, pp. 254–256, 1946.

[51] R. D. Straw, ed., *The ARRL Antenna Book*. ARRL, 2007.

[52] H. Yagi and S. Uda, “Projector of the sharpest beam of electric waves,” *Proceedings of the Imperial Academy*, vol. 2, no. 2, pp. 49–52, 1926.

[53] C. A. Balanis, *Antenna Theory: Analysis and Design*. John Wiley & Sons, 2016.

[54] P. Viezbicke, “NBS Technical Note 688: Yagi Antenna Design,” *US Department of Commerce, Washington, DC*, 1976.

[55] C. A. Balanis, *Modern Antenna Handbook*. John Wiley & Sons, 2011.

[56] Amateur Radio in International Space Station (ARISS). `https://www.ariss.org/`, accessed 2020-05-01.

[57] E. J. Wilkinson, “An N-way hybrid power divider,” *IRE Transactions on Microwave Theory and Techniques*, vol. 8, pp. 116–118, Jan. 1960.

[58] D. M. Pozar, *Microwave Engineering*. John Wiley & Sons, 2009.

[59] K. Fujimoto and H. Morishita, *Modern Small Antennas*. Cambridge University Press, 2013.

[60] Würth Elektronik, “WE-STAR-TEC Snap Ferrite with Safety Key Technology,” 2020. `https://www.we-online.com/catalog/en/WE-STAR-TEC/`, accessed 2020-07-01.

[61] Heavens Above, “ISS Pass Details.” `https://www.heavens-above.com/`, accessed 2020-08-04.